Tampere University

Iida Kangashaka

THE BENDING, SHEAR AND TORSION RESISTANCES OF PARTIALLY PROTECTED BEAMS IN FIRE

Faculty of Built Environment
Master's Thesis
May 2019

ABSTRACT

Iida Kangashaka: The bending, shear and torsion resistances of partially protected beams in fire
Master's Thesis
Tampere University
Master's Degree Programme in Civil Engineering
May 2019

Intumescent coating is often used as fire protection on steel members due to its attractive appearance and how easy it is to apply. In some cases, the member can be only partially covered. Examples of these cases are when the member is coated on site, but a structure has been installed adjacent to the member before the coating happens. Other examples are when the member has been fully coated but the coating is damaged or when a secondary beam is joined to the studied beam on its span and the joint is left unprotected.

The previous research on this subject has mainly been about the increase in temperature caused by the unprotected part of the beam. To address this, Hautala et al. conducted a simulation study on the bending resistance of a partially protected IPE 200 beam in fire. This thesis aims to expand on their results and produce heating time-resistance curves for bending, shear and torsion to aid in designing steel structures.

FEM models are made to determine the bending, shear and torsion resistances of partially protected IPE 200 and HEA 200 beams during fire. The models are made for fully protected, partially protected and unprotected beams so that the results can be compared. The expansion of the intumescent coating is not explicitly modeled but is taken into account by using an effective thermal conductivity. The temperature results are validated using experimental and simulation results from previous research.

The results were bending, shear and torsion resistance curves as functions of the heating time. They show that additional intumescent coating of the partially protected beam mainly affects the resistances in the middle of the fire when comparing to the unprotected beam.

Keywords: Unsymmetric fire, intumescent coating, steel structure, FEM, bending, shear, torsion

TIIVISTELMÄ

Iida Kangashaka: Osittain palosuojattujen teräspalkkien taivutus-, leikkaus- ja vääntökestävyydet palossa
Diplomityö
Tampereen yliopisto
Rakennustekniikan diplomi-insinöörin tutkinto-ohjelma
Toukokuu 2019

Lämpölaajenevaa palomaalia käytetään usein teräsrakenteiden palosuojauksessa johtuen sen asentamisen helppoudesta ja ulkonäkösyistä. Joissain tapauksissa rakenne saattaa olla vain osittain suojattu. Yksi esimerkki tällaisesta on tapaus, jossa palkkia vasten asennettu rakenne estää kaikkien pintojen suojauksen. Muita esimerkkejä ovat kokonaan suojatun palkin maalin vaurioituminen tai sekundaarisen palkin liittäminen tutkittuun palkkiin, kun liitos jätetään suojaamatta.

Aikaisempi tutkimus tähän aiheeseen liittyen on käsitellyt lähinnä vain palkin suojaamattoman osan aiheuttamaa teräksen lämpötilan kasvua. Täydentääkseen tutkimusta, Hautala et al. tutkivat simuloimalla osittain suojatun IPE 200 -palkin taivutuskestävyyttä palossa. Tämä työ pyrkii laajentamaan heidän tuloksiaan ja tuottamaan lämmitysaika-kestävyys käyrät taivutukselle, leikkaukselle ja väännölle, joita voidaan käyttää teräsrakenteiden suunnittelussa.

Osittain suojattujen IPE 200 - ja HEA 200 -palkkien taivutus-, leikkaus- ja vääntökestävyyksien selvittämiseksi rakennetaan FEM-mallit. Mallit tehdään täysin suojatuille, osittain suojatuille ja suojaamattomille palkeille tulosten vertailua varten. Lämpölaajenevan palomaalin laajenemista ei mallinneta suoraan, vaan se otetaan huomioon käyttämällä efektiivistä lämmönjohtavuutta. Lämpötilatulokset osoitetaan kelvollisiksi aiemmasta tutkimuksesta löytyvien simulaatio- ja testitulosten avulla.

Tuloksina saatiin taivutus-, leikkaus- ja vääntökestävyyskäyrät lämmitysajan suhteen. Niistä ilmenee, että osittain suojatun palkin ylimääräinen palomaali vaikuttaa kestävyyksiin lähinnä palon puolessa välissä, kun verrataan suojaamattomaan palkkiin.

Avainsanat: Epäsymmetrinen palo, lämpölaajeneva palomaali, teräsrakenne, FEM, taivutus, leikkaus, vääntö

PREFACE

This thesis was written for the Faculty of Built Environment of Tampere University between July 2018 and May 2019. Professor Sami Pajunen supervised the project. The examiners of the thesis were Professor Sami Pajunen and Professor Mikko Malaska.

I would like to thank Professor Sami Pajunen for providing an interesting subject, as well as giving valuable guidance and support. I would also like to thank Janne Hautala for helping me get started with ANSYS Workbench and answering all my questions about it along the way.

Finally, I want to express my gratitude to my family. To my siblings Eveliina and Nestori for patiently listening to me talk about models I had made and was proud of. And especially to my parents Hannele and Kauko for pushing me to work even when I struggled. Couldn't have done it without you.

Tampereella, 4.5.2019

Iida Kangashaka

CONTENTS

TABLE OF FIGURES

LIST OF ABBREVIATIONS AND SYMBOLS

IC	intumescent coating
ISO-834	standard temperature-time curve for fire according to EN 1991-1-2
h	height of the cross section
$M_{fi,t,Rd}$	design bending resistance at time t for an uneven temperature distribution
t	time
A_i	area of element i
z_i	distance of the center of the elemental area i from the plastic neutral axis
$k_{y,\theta i}$	reduction factor for yield strength of element i at temperature θ_a
$f_{y,i}$	yield strength of the element i
$\gamma_{M,fi}$	partial factor in fire
$M_{fi,\theta,Rd}$	design bending resistance of the beam with the uniform temperature θ_a at time t the profile would have if it wasn't thermally influenced by supports or a composite/concrete slab
κ_1	adaptation factor for uneven temperature across the cross section
κ_2	adaptation factor for uneven temperature along the beam
$k_{y,\theta}$	reduction factor for yield strength at temperature θ_a
γ_{M0}	partial factor
$M_{pl,Rd}$	plastic bending resistance at room temperature
W_{pl}	plastic section modulus of the cross section
f_y	yield strength of steel
$V_{fi,t,Rd}$	design shear resistance of the cross section at time t
$V_{pl,Rd}$	shear resistance at room temperature
θ_{web}	average temperature of the web at time t
$k_{y,\theta,web}$	reduction factor for yield strength at temperature θweb
A_v	shear area
A	area of the beam cross section
b	width of the cross section
t_f	flange thickness
t_w	web thickness
r	root radius
η	factor according to EN 1993-1-5
h_w	height of the web
α	thermal expansion factor
ψ	porosity
λ_{eq}	equivalent thermal conductivity
λ_p	thermal conductivity of the trapped gas inside the pores
λ_{IC}	thermal conductivity of IC at room temperature
σ	Stefan-Boltzmann constant
θ_{IC}	temperature of intumescent coating
d_p	diameter of the pores
λ_{eff}	effective thermal conductivity
E_{IC}	Young's modulus of intumescent coating
υ_{IC}	Poisson's ratio of intumescent coating
ρ_{IC}	density of intumescent coating
E_a	Young's modulus of steel

ρ_a	density of steel
υ_a	Poisson's ratio of steel
α_c	coefficient of heat transfer by convection
ε_{IC}	emissivity of intumescent coating
ε_a	emissivity of steel
L	length of a beam
φ_z	rotation on the free end of a beam around the z-axis
v	displacement on the free end of a beam
F	force on the free end of the beam
M	maximum bending moment of a beam
Q	maximum shear force of a beam
τ_{avg}	average shear stress on the cross section
σ_{avg}	average bending stress on the cross section
I_y	second moment of the cross-section
z	longest distance between the neutral axis and an edge of the cross section
φ_x	rotation on the free end of a beam around the x-axis

1. INTRODUCTION

In some situations, intumescent coating doesn't fully surround a profile. This can happen when fire proofing happens on site and the profile cannot be fully protected due to an adjacent structure covering a face of the profile. This is the case if roofing has already been installed on beams, or wall elements have been attached to columns before the intumescent coating is applied. Damaged intumescent coating can also lead to an inadequately fire proofed profile. A third instance of improperly fire protected steel profiles can occur if a secondary beam is joined to a primary beam at its span. According to [9], [10] and [11] the joints can in some cases be left unprotected due to the time-consuming nature of applying intumescent coating on site. In case of fire, this would increase the temperature of the beam near the joint. This study focuses on the first example.

Eurocode EN 1993-1-2 covers the fire design for steel structures. Unfortunately, the standard only addresses fire design with passive methods of fire protection [32]. When studying bending, the only way to take into account the non-uniform temperature gradient caused by uneven coating according to the Eurocode is to calculate the bending resistance as a sum of the parts with different temperature, or by using an adaptation factor [32]. The first method would be too time consuming for a continuous temperature gradient and the adaptation factor doesn't cover the situation studied in this thesis. For shear resistance a method using an average temperature of the web of the cross section is offered [32], which is not an accurate enough method for this study. Nothing is mentioned about calculating torsion resistance for uneven temperature gradients. This is why the behavior of intumescent coatings and the effect of an uneven temperature distribution have been researched extensively. Di Blasi and Branca [12] have created a mathematical model for the foaming mechanism of intumescent coating in fire. Equivalent thermal conductivity of intumescent coating, when the foaming mechanism is also modelled, has been researched by [28], [41], [14], [24], [47] and [46]. Models for effective thermal conductivity have been created by [5], [37] and [41]. When using the effective thermal conductivity for intumescent coating, its foaming is not explicitly modelled, but the expansion is taken into account when calculating the thermal conductivity. Ways to calculate a constant thermal conductivity of intumescent coating have likewise been determined by [21], [22] and [45]. Schaumann et al. [29] have investigated the temperature gradient of a steel profile covered by intumescent coating supporting a trapezoidal steel sheet, which partially prevents the foaming process on the upper face of the profile. They have also created a simplified method for calculating the temperature of the profile without modeling the foaming mechanism [28]. Investigations on the behavior of steel columns in unsymmetrical

fire have been conducted by [1] and [40], and of concrete filled steel tube columns in unsymmetrical fire by [16], [18], [44] and [43].

Of the previous research presented almost all of the research done on columns includes structural analysis, except for [40]. However, in most of the cases the faces of the columns that were not protected with intumescent coating were against a concrete wall or some other type of insulating material, except for the columns in [1]. The papers written on intumescent coating all have either a beam or a steel plate as the base for the coating. They don't include a structural analysis, and most of them have the steel profile or plate completely fire protected, except for the one by Schaumann et al. [29], where the top flange is partially unprotected. As can be seen, the research for beams so far has been mostly about the performance of the coating, whereas for columns there has been more interest for structural performance as well. To remedy this Hautala et al. [17] have conducted a study that solves the bending resistance of an IPE 200 member covered with intumescent coating on all sides except for the top flange, which is left unprotected. The study was done as a simulation using ANSYS Workbench and validated with the data from an investigation by Tabeling [39]. The model used effective thermal conductivity for the intumescent coating, for which the mathematical model was taken from research by Schaumann et al. [28]. Hautala et al. studied the bending resistance of a fully protected profile, a fully unprotected profile and a profile, which was protected partially as described before, at different temperatures. The bending resistances of the coating cases as a function of temperature were then compared at different heating times. It was found that the differences in fire protection have the most effect on the bending resistance at the midparts of the fire. The bending resistance of the fully protected member was halved at around 31 minutes, the resistance of the partially protected member was halved at about 17 minutes and the resistance of the unprotected profile was halved at approximately 10 minutes from the beginning of the fire. This shows that a partially protected profile definitely doesn't last as long in a fire as a fully protected profile, but it would also be wasteful to expect a partially protected profile to fail when an unprotected profile would.

The present study is based on Hautala et al.'s work and aims to expand on it. The profiles examined are common open profiles IPE 200 and HEA 200. Closed profiles are excluded from this study due to the difficulty in correctly simulating the radiation and convection inside the profile. Bending, shear and torsion resistances are solved for both profiles. Each of the profiles is simulated with three different levels of fire protection in three different loading cases. For the partially protected profile the outer surface of the upper flange of IPE and HEA is left unprotected. The thermal conductivity of the intumescent coating is calculated using the same model of thermal conductivity by Schaumann et al. [28] that Hautala et al. used. The simulations are done using ANSYS Workbench 19.2 [3].

This paper is divided into four parts introducing the materials, the design methods presented in the Eurocode, the used FEM models and finally the results. The first part introduces the basics of intumescent coating and the effect of the uneven temperature on steel

profiles. The second part further explains the methods offered in Eurocode for calculating resistances for uneven temperature gradients. The third part includes the created material models for steel and intumescent coating, the principles the different model types are based on, the meshing and finite elements of the models. The models are then validated with experimental data from previous research. Finally, the fourth part describes the temperature curves of the profiles over time and the results of the case studies.

2. THE EFFECT OF FIRE ON THE MATERIALS

2.1 Intumescent coating

To induce intumescence, it is generally agreed that three components are needed: a charring agent (carbonific), an acid catalyst and a blowing agent (spumific) [19][42][20][24][22][46]. Typically, intumescent systems have ammonium polyphosphate as their acid catalyst, melamine (as well as its derivatives) as a blowing agent, and, as a charring agent, pentaerythritol and its derivatives [19][22]. In order for the system to be used in paints, it needs to be bound in a resin [19][24][22][46]. Most common resins are polyurethane, epoxy and polypropylene [24].

The reactions caused by heat on an intumescent coating according to [20][15][24][22][46] are:

1. The polymer matrix (resin) is melted into a viscous liquid.
2. The acid catalyst decomposes. The resulting acid dehydrates the charring agent. This is to prepare the carbon-rich carbonific for charring later on in the process.
3. The blowing agent releases a large amount of gas into the liquid. Some of this gas gets trapped in the matrix, which causes bubbles to form in the fluid. This leads to the swelling of the coating.
4. When the temperature is high enough the liquid begins to harden through cross-linking and releases surplus volatiles.
5. Finally, the char oxidizes further, creating an inert and highly porous layer.

The timing of the gas formation in relation to the melting of the resin is very important. If the gas starts to form too early when the polymer is still too viscous the bubbles cannot be created. In this case the gas merely diffuses through the polymer. If gas forms too late, the fluid has already begun to solidify into a char, and bubbles can't be created. If the polymer matrix melts into a fluid with a low enough viscosity the bubbles can grow too big. This leads to char that is fragile and a poor insulator. [2][24]

2.2 The effects of uneven temperature on steel

In this thesis the consequences of using intumescent coating to protect steel beams on all other sides except the top surface are studied. The uneven temperature gradient caused by this affects the mechanical properties of the steel beams. The mechanical properties included in this study as temperature-dependent are yield strength, Young's modulus and tangent modulus.

The Eurocode [32] presents values for the yield strength as a function of temperature. The value of the yield strength until 400 °C remains the same as the value at room temperature. After that it begins to decrease until it reaches 0 MPa at 1200 °C. This applies to all

steel grades. The steel grade used in this study is S 355, and its yield strength is further discussed in later chapters.

An uneven temperature gradient on a profile is caused by either adding a heat sink, having a fire on one side of the profile or removing fire protection. A member is connected to a heat sink when it is adjacent to a concrete or composite structure. This happens when a steel beam carries a concrete or composite slab, or when a steel column is placed next to a concrete or composite wall. In fire the steel member quickly conducts the heat to the interface between the steel and the concrete or composite structure. From there the heat sink absorbs some of the heat and cools the steel member down. The effect of the uneven temperature distribution caused by a heat sink on columns have been studied by [18] and [40].

Another reason for an unsymmetrical temperature gradient on a cross section is if the fire is only on one side of the member. This happens if the frame of a wall or a floor is made of steel channel columns or beams. If a fire happens on only one side of the wall or floor, the temperature of one flange rises faster than the temperature of the other, leading to a non-symmetrical temperature gradient. The effect of the uneven temperature caused by the one-sided fire on the resistance of the steel frame has been studied in [23], [34], [13] and [4].

A third situation where an uneven temperature gradient is created on a steel cross section is if some of the fire proofing is removed on some surfaces of the profile. This can happen if a structure has been installed next to the member before it is coated, so that the paint cannot be applied on all surfaces. However, the adjacent structure must allow the fire onto the unprotected surface of the member. An example of this is when a trapezoidal steel sheet is installed on a beam before the beam is coated. The unprotected surface will cause some parts of the member to heat up faster than the protected parts do, leading to an uneven temperature gradient. This has been studied before by [17] and [25], and it is the subject of this thesis. A non-symmetrical temperature distribution can be caused by damaged fire protection as well.

Since the yield strength of steel depends on the temperature, the uneven temperature distribution also produces an uneven yield strength distribution. Due to the lower yield strengths the stress causes the beam to yield sooner than it would at room temperature. The uneven yield strength gradient causes the top part of the profile to start being plasticized earlier than the bottom part. This leads to the beam to reach its yield strength when the bottom part still has some capacity left.

However, a plastic strain of 0.2 % is allowed before the beam reaches its resistance. Figure 1 shows as an example a beam and its bending stress distribution when it has just reached its yield strength (a), and when it has been allowed a 0.2 % plastic strain (b).

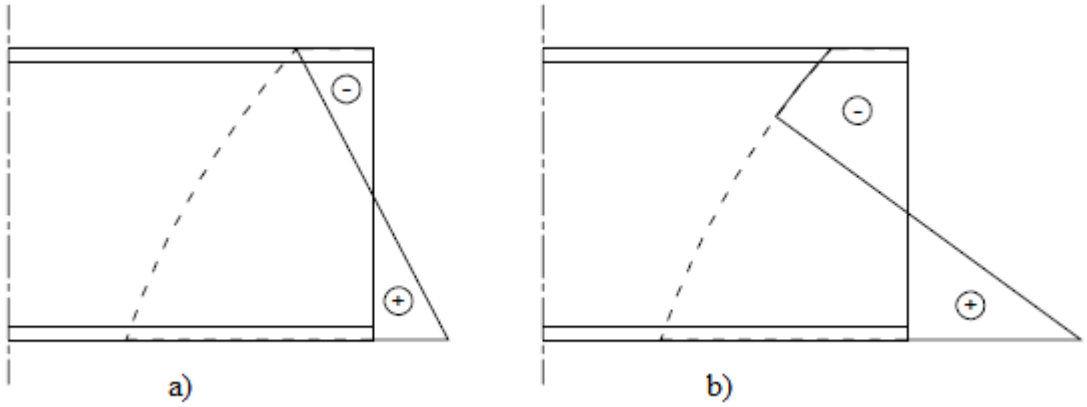

Figure 1. *a) Maximum bending stress of a beam, when no plastic strain is allowed. b) Bending stress of a beam when 0.2 % of plastic strain is allowed*

The dashed line shows the yield strength over the cross section. In Figure 1b the top parts of the profile have started to yield, which causes the neutral axis to move lower and allows more of the bottom part's capacity to be used.

3. RESISTANCES ACCORDING TO EUROCODE

The Eurocode only covers passive fire protection methods, so methods with a changing thermal conductivity are not allowed [32, 1.1.2]. There is no method presented in EN 1993-1-2 for calculating an uneven temperature gradient for the profile of a steel beam. However, there are some methods offered in the Eurocode for calculating resistances for an uneven temperature distribution. However, since no method is given for calculating an unsymmetrical temperature gradient, it must be determined by using some other approach not given in the Eurocode.

The first method for calculating the bending resistance for a cross section with an uneven temperature distribution is [32, Equation 4.9]

$$M_{fi,t,Rd} = \sum_{i=1}^{n} A_i z_i k_{y,\theta i} f_{y,i} / \gamma_{M,fi} \quad (1)$$

where $M_{fi,t,Rd}$: design bending resistance at time t for an uneven temperature distribution [Nm]
A_i: area of element i [m^2]
z_i: distance of the center of the elemental area i from the plastic neutral axis [m]
$k_{y,\theta i}$: reduction factor for yield strength of element i at temperature θ_a [-]
$f_{y,i}$: yield strength of the element i [Pa]
$\gamma_{M,fi}$: partial factor in fire [-]

With a continuous temperature gradient this method would quickly become far too time consuming to be practical. This is especially the case when the temperature gradient cannot be assumed linear.

There is also a simpler method for calculating bending resistance in profiles with uneven temperature distributions that uses adaptation factors. Using this method, the resistance is calculated according to [32, Equation 4.10]

$$M_{fi,t,Rd} = M_{fi,\theta,Rd} / (\kappa_1 \kappa_2) \quad (2)$$

where $M_{fi,t,Rd}$: design bending resistance at time t for an uneven temperature distribution [Nm]
$M_{fi,\theta,Rd}$: design bending resistance of the beam with the uniform temperature θ_a at time t the profile would have if it wasn't thermally influenced by supports or a composite/concrete slab [Nm]
κ_1: adaptation factor for uneven temperature across the cross section [-]
κ_2: adaptation factor for uneven temperature along the beam [-]

The design bending resistance for a profile with a uniform temperature gradient is determined by [32, Equation 4.8]

$$M_{fi,\theta,Rd} = k_{y,\theta}\left[\frac{\gamma_{M0}}{\gamma_{M,fi}}\right]M_{pl,Rd} \quad (3)$$

where $M_{fi,\theta,Rd}$: design bending resistance for a uniform temperature gradient [Nm]
$k_{y,\theta}$: reduction factor for yield strength at temperature θ_a [-]
γ_{M0}: partial factor [-]
$\gamma_{M,fi}$: partial factor in fire [-]
$M_{pl,Rd}$: plastic bending resistance at room temperature [Nm]

Since both IPE 200 and HEA 200 profiles have a class 1 cross section [31, Table 5.2], the bending resistances at room temperature around one principal axis are calculated according to [31, Equation 6.13] as

$$M_{pl,Rd} = \frac{W_{pl}f_y}{\gamma_{M0}} \quad (4)$$

where $M_{pl,Rd}$: plastic bending resistance of the cross section [Nm]
W_{pl}: plastic section modulus of the cross section [m^3]
f_y: yield strength of steel [Pa]
γ_{M0}: partial factor [-]

The adaptation factor κ_1 only has values for two different situations: when the beam is unprotected and exposed to fire on three sides while the fourth side is covered by a composite or concrete slab, or the same situation but the beam is protected. This is not enough for the requirements of the present study.

Not much is said about shear resistance of beams in fire. Eurocode offers an equation for calculating the design shear resistance using an average temperature of the web of the cross section in [32, Equation 4.16]

$$V_{fi,t,Rd} = k_{y,\theta,web}V_{pl,Rd}\left[\frac{\gamma_{M0}}{\gamma_{M,fi}}\right] \quad (5)$$

where $V_{fi,t,Rd}$: design shear resistance of the cross section at time t [N]
$V_{pl,Rd}$: shear resistance at room temperature [N]
θ_{web}: average temperature of the web at time t [°C]
$k_{y,\theta,web}$: reduction factor for yield strength at temperature θ_{web} [-]
γ_{M0}: partial factor [-]
$\gamma_{M,fi}$: partial factor in fire [-]

The plastic shear resistance at room temperature is calculated according to [31, Equation 6.18]

$$V_{pl,Rd} = \frac{A_v(f_y/\sqrt{3})}{\gamma_{M0}} \quad (6)$$

where $V_{pl,Rd}$: plastic shear resistance of the cross section [N]
A_v: shear area [m^2]
f_y: yield strength of steel [Pa]
γ_{M0}: partial factor [-]

The shear area of rolled I- and H-sections is determined according to [31, 6.2.6 (3a)] when the load is parallel to the web.

$$A_v = max\left(A - 2bt_f + (t_w + 2r)t_f;\ \eta h_w t_w\right) \quad (7)$$

where A_v: shear area [m^2]
A: area of the beam cross section [m^2]
b: width of the cross section [m]
t_f: flange thickness [m]
t_w: web thickness [m]
r: root radius [m]
η: factor according to [33] [-]
h_w: height of the web [m]

Since the shear resistance equation uses an average temperature it could be used in cases with an uneven temperature gradient. However, it is an approximation, and the present study is looking to find more accurate results. EN 1993-1-2 says nothing about torsion resistance for beams in fire.

4. FEM-MODEL

4.1 Material models and fire model

The effective thermal conductivity of intumescent coating used in this study is calculated using Schaumann et al.'s [28] numerical approach to calculate the equivalent thermal conductivity and then divided by the thermal expansion factor α. The definition of the expansion factor is the thickness of the foam at time step i divided by the original thickness. It was derived from a series of tests on different types of intumescent coating done by Schaumann et al. [28]. The results can be seen in Figure 2. The thickness of intumescent coating increases until about 520 °C, after which it begins to shrink.

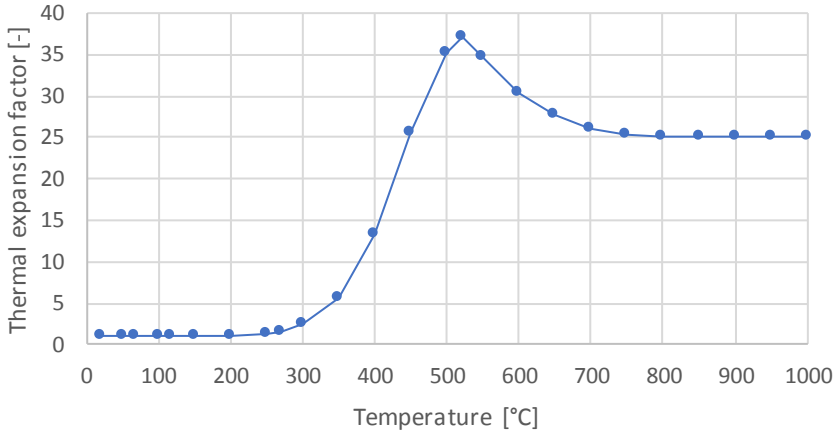

Figure 2. *Thermal expansion factor of intumescent coating as a function of temperature [28, Fig. 3a]*

The porosity of the intumescent coating is the ratio between the volume of the gas in the pores of the foam and the volume of the entire foam [28]. It is described as follows.

$$\psi(\theta) = \frac{\alpha - 1}{\alpha} \tag{8}$$

where $\psi(\theta)$: porosity [-]
α: thermal expansion factor [-]

The equivalent thermal conductivity of intumescent coating is calculated according to Equation 9 [28]. This thermal conductivity is used when the expansion of the intumescent coating is modeled explicitly.

$$\lambda_{eq}(\theta) = \psi\left(\lambda_p + 4\sigma\theta_{IC}^3 d_p\right) + (1-\psi)\lambda_{IC} \quad (9)$$

where
- λ_{eq}: equivalent thermal conductivity [W/(mK)]
- ψ: porosity [-]
- λ_p: thermal conductivity of the trapped gas inside the pores [W/(mK)]
- σ: Stefan-Boltzmann constant [W/(m^{2}K^4)]
- θ_{IC}: temperature of IC [K]
- d_p: diameter of the pores [m]
- λ_{IC}: thermal conductivity of IC at room temperature [W/(mK)]

The gas trapped in the pores is assumed to be nitrogen in this study. Tabeling [39] has conducted tests on intumescent coating and based on the results the thermal conductivity of intumescent coating at room temperature is λ_{IC} = 0.45 W/(mK). The pore size is fixed at d_p = 1.2 mm [28].

Using the equivalent thermal conductivity by Schaumann et al., an effective thermal conductivity is described in the following Equation 10 [17]. This thermal conductivity value takes the expansion of the intumescent coating into account, and so it does not need to be modeled.

$$\lambda_{eff} = \frac{\lambda_{eq}}{\alpha} \quad (10)$$

where
- λ_{eff}: effective thermal conductivity [W/(mK)]
- λ_{eq}: equivalent thermal conductivity [W/(mK)]
- α: thermal expansion factor [-]

The difference between equivalent and effective thermal conductivity can be seen in Figure 3. At lower temperatures the thermal conductivities are very similar. Once the temperature rises above approximately 150 °C the conductivities start to differ. This is due to the intumescent coating beginning to expand, which can also be seen in Figure 2 as the increasing value of the thermal expansion factor. The equivalent thermal conductivity is at its lowest at 400 °C, after which it begins to increase. After 500 °C the effective thermal conductivity increases as well towards the higher temperatures, but the increase happens significantly slower. This well demonstrates the importance of intumescent coating's ability to expand and its effect on the coating's thermal insulation properties.

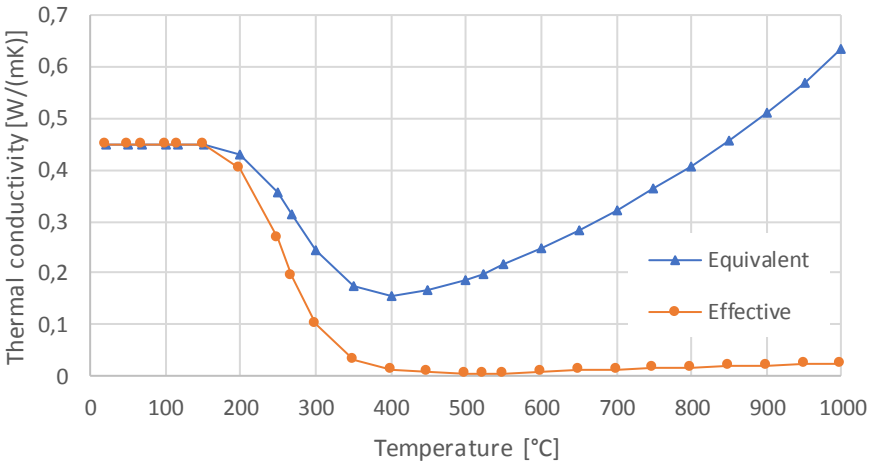

Figure 3. *Comparison of the equivalent and effective thermal conductivities of intumescent coating*

The stress analysis is done so that the intumescent coating body is suppressed. Since this study aims to find the shear, bending and torsion resistances of the steel beams, the intumescent coating is suppressed so as to not influence the results. However, ANSYS Workbench requires the mechanical properties for the coating to be defined. Therefore, the Young's modulus of the intumescent coating is set to $E_{IC} = 1$ N/mm^2 and Poisson's ratio is $\upsilon_{IC} = 0.0$. With these values the impact of the intumescent coating is insignificant. The mechanical behavior of the coating is assumed to be linear elastic. The specific heat of intumescent coating is shown in Figure 4 and the density is assumed to be constant $\rho_{IC} =$ 1400 kg/m^3. [28]

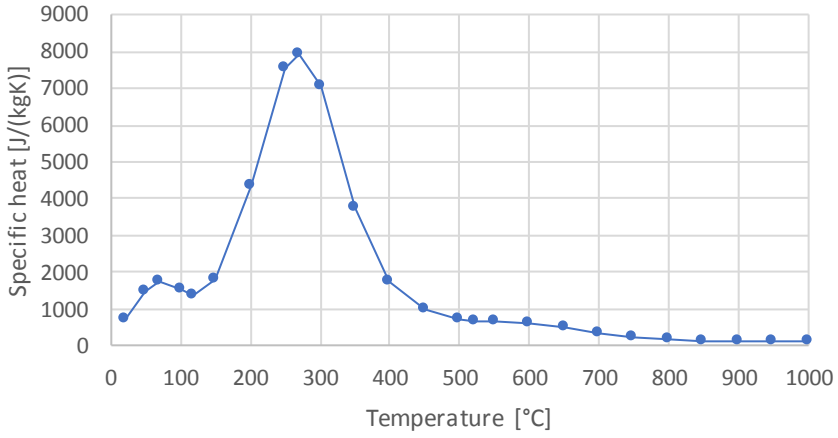

Figure 4. *Specific heat of intumescent coating [28, Fig. 3b]*

The thermal material properties of steel at elevated temperatures are from [32]. They are shown in Figure 5 and Figure 6.

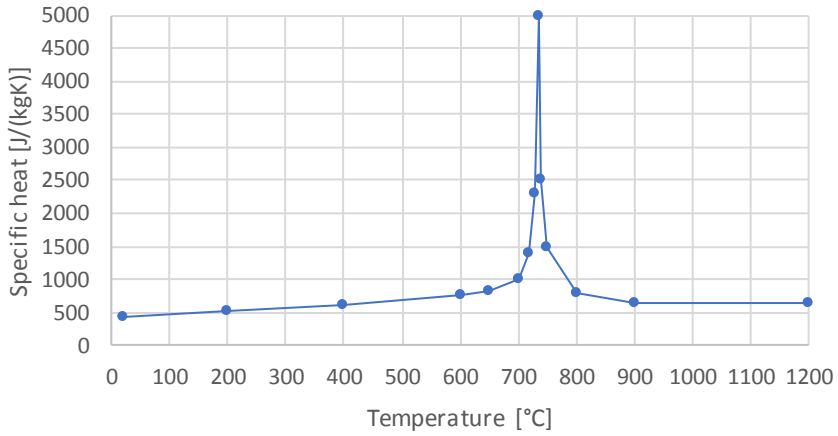

Figure 5. *Specific heat of steel S 355 as a function of temperature*

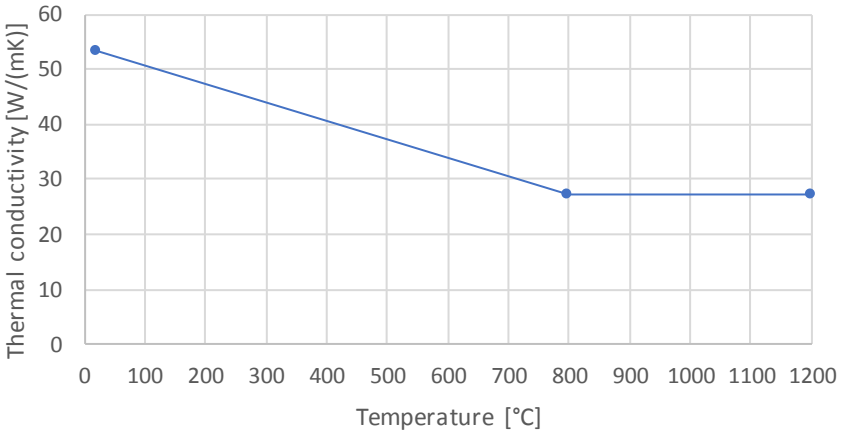

Figure 6. *Thermal conductivity of steel S 355 as a function of temperature*

The mechanical material properties for steel at elevated temperatures are from [32]. Steel is here assumed to be a linear elastic, linear strain hardening material. Young's modulus E_a and yield strength f_y as a function of temperature are from [32] and are shown in Figure 7 and Figure 8. Tangent modulus is calculated according to [33] as $E_a/100$. The temperature independent density of steel is $\rho_a = 7850$ kg/m^3 according to [32], and Poisson's ratio is $\upsilon_a = 0.3$ according to [31]. The shear strength is $0.6f_y$ according to [27].

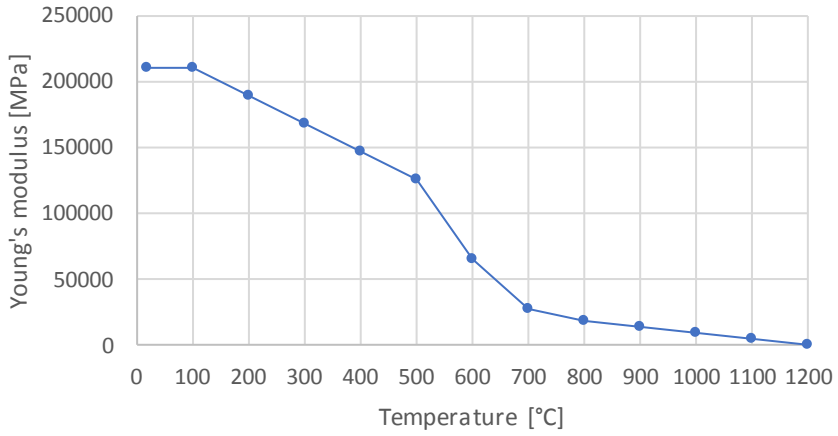

Figure 7. *Young's modulus of steel S 355 as a function of temperature*

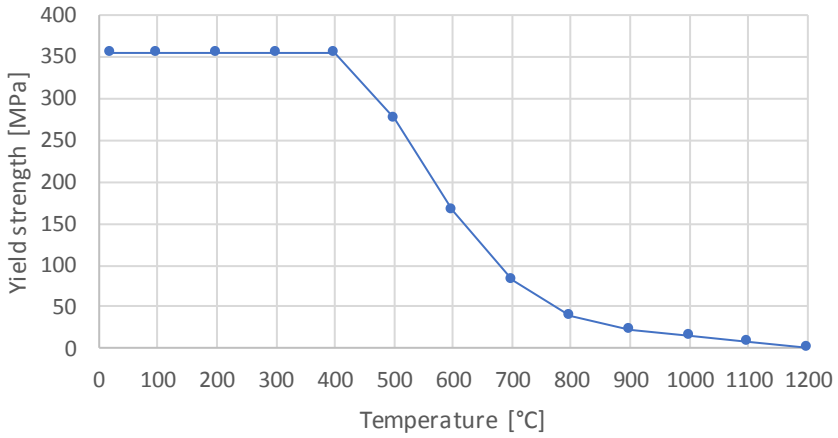

Figure 8. *Yield strength of steel S 355 as a function of temperature*

The fire model used is the ISO-834 standard fire curve with a coefficient of heat transfer by convection of $\alpha_c = 25$ W/(m^{2}K) [30]. The emissivity of the intumescent coating surface is $\varepsilon_{IC} = 0.8$ according to [39] and the emissivity of the unprotected steel surface is $\varepsilon_a = 0.7$ according to [32].

4.2 Simulation

4.2.1 Model for bending

The beam used for bending resistance analyses is a cantilever beam with a length L of 0.2 m. The bending moment resistance is determined from the support moment caused by a rotation φ_z around the z-axis introduced on the free end of the beam. The beam and rotation are shown in Figure 9.

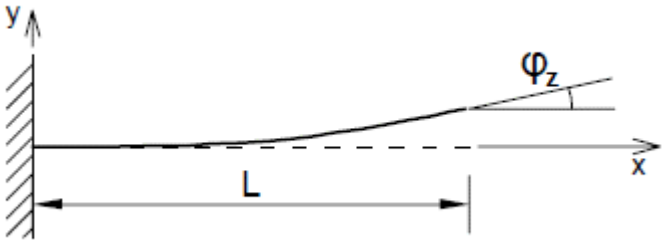

Figure 9. *Mechanical model for a beam loaded with a rotation around the z-axis at the free end*

Three separate models are made: one where the beam is fully protected, one where the beam is only partially protected and one where the beam is unprotected. For each model a thermal analysis is performed where a time dependent temperature according to the ISO-834 fire curve is applied on the sides of the beam. After this, 14 separate static structural analyses are performed for each level of fire protection. For each analysis, a temperature gradient at heating time t is applied as a body load on the beam. The heating times are t = 0 s, 300 s, 600 s, 900 s, 1200 s, 1500 s, 1800 s, 2100 s, 2400 s, 2700 s, 3000 s, 3300 s and 3600 s, as well as 450 s since for partially protected beams adding a resistance value at that time often changes the shape of the resistance curve quite significantly.

The model is divided into two bodies, steel and intumescent coating. In the structural analyses the intumescent coating-body is suppressed. The small added resistance caused by the coating is not of interest in this study, so it is left out of the calculations. One end of the beam is supported so that neither translation nor rotation are allowed. On the free end, translation is not allowed along the z-axis and rotation is forbidden around x- and y-axes. The beam is loaded with the rotation for 0.6 s which is divided into time steps of 0.02 s. The rotation changes during the loading time linearly from 0 to 0.6 degrees. The moment reaction at the supported end of the beam is measured as a function of time. The plastic strain of the flanges is also measured as a function of time. The moment reaction values are then plotted as a function of the rotation for all heating times.

4.2.2 Model for shear

A cantilever beam is used for determining the shear resistance curves as well. The length L of the beam must be made so short that it eliminates the effect of bending moment on the shear failure of the beam. The shear resistance is determined by applying a displacement v in y-direction on the free end of the beam and measuring the force reaction caused on the supported end. The beam and displacement are shown in Figure 10.

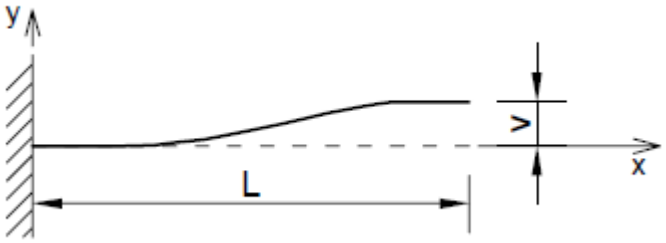

Figure 10. *Mechanical model for a beam loaded with a displacement in y-direction at the free end*

To determine an appropriate length for the beam, a force F is applied to the free end of the beam. This is shown in Figure 11. The maximum bending moment M caused by the force is at the supported end of the beam and the shear force is at its maximum value Q along the entire length of the beam.

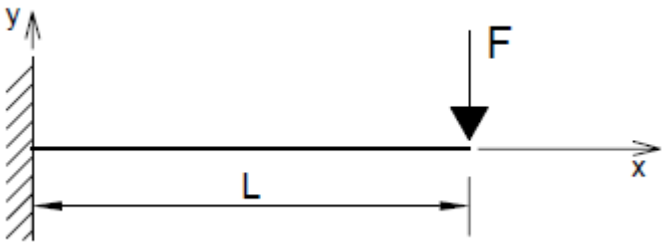

Figure 11. *Mechanical model for a beam loaded with a force in y-direction at the free end*

The average shear stress τ_{avg} and average bending stress σ_{avg} are calculated from the maximum bending moment and shear force values according to Equation 11 and Equation 12.

$$\tau_{avg} = \frac{Q}{A} \tag{11}$$

where τ_{avg}: average shear stress on the cross section [Pa]
Q: maximum shear force of the beam [N]
A: area of the beam cross section [m^2]

$$\sigma_{avg} = \frac{1}{2}\frac{M}{I_y}z \tag{12}$$

where σ_{avg}: average bending stress on the cross section [Pa]
M: maximum bending moment of the beam [Nm]
I_y: second moment of the cross-section [m^4]
z: longest distance between the neutral axis and an edge of the cross section [m]

To compare the stresses, a bending stress to shear stress ratio is calculated. The ratio is calculated with Equation 13 when for a cantilever beam the maximum shear force $Q = F$ and the maximum bending moment is $M = FL$. The results for all three profiles are shown in Table 1.

$$\frac{\sigma_{avg}}{\tau_{avg}} * 100\% = \frac{M*z}{2*I_y}\frac{A}{Q} * 100\% = \frac{FLzA}{2I_yF} * 100\% = \frac{LzA}{2I_y} * 100\% \qquad (13)$$

Table 1. *The bending stress to shear stress ratio for IPE 200 and HEA 200 for different beam lengths*

	IPE 200	HEA 200
L m	ratio %	ratio %
0.200	146.6	138.5
0.100	73.3	69.3
0.020	14.7	13.9
0.010	7.3	6.9
0.005	3.7	3.5

To make sure the shear stresses are dominant, a member length is chosen so that the bending stress to shear stress ratio is below 10 %. For this reason, the chosen length is 10 mm for both profiles. This way the loading on the beam can be assumed to be pure shear force.

As for the model for bending resistance, three separate models for the three levels of fire protection are made. The thermal analyses are conducted as before and the temperature gradients at different heating times are applied on the beams in the static structural analyses as stated earlier.

In the structural analyses the intumescent coating is again left out. As before, the beam is supported from one end so that translation and rotation are not possible. At the free end the beam is supported in a way that doesn't allow for rotation around any axis or translation along the z-axis. The beam is once again loaded for 0.6 s with time steps of 0.02 s, except for the partially protected HEA 200 beam at heating times 600 s, 900 s, 1200 s, 1500 s and 1800 s. This is due to the fact that for these cases the plastic strain did not begin until after 0.6 s. The displacement introduced on the free end of the beam increases linearly from 0 m to 0.06 mm over the 0.6 s. The force reaction at the supported end of the beam and the plastic strain at the web of the beam are both measured as a function of time. The shear force reaction is plotted as a function of the displacement for all heating times. These plots show the force values for the displacement during the 0.6 s.

4.2.3 Model for torsion

As for bending resistance, a cantilever beam of length L = 0.2 m is used. A rotation φ_x around the x-axis is introduced at the free end of the beam and the torsion moment resistance is calculated from a moment reaction at the supported end. The beam and rotation are shown Figure 12.

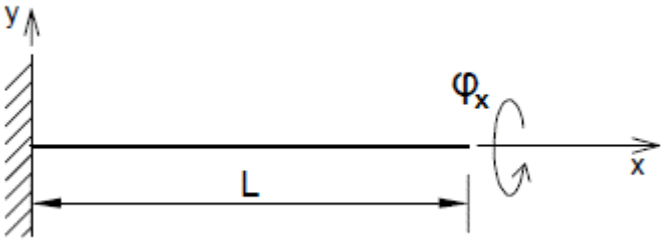

Figure 12. *Mechanical model for a beam loaded with a rotation around the x-axis at the free end*

The three models for the different levels of fire protection are created and the thermal analyses are done as before. The temperature gradients at different heating times are applied to the beams in the structural analyses, as mentioned earlier.

The intumescent coating is again suppressed during the static structural calculations. A fixed support is applied on one end of the beam to prevent all translation and rotation at that end. The beam is loaded for 0.6 s with time steps of 0.02 s. A rotation around the x-axis is applied to the free end of the beam. The rotation changes linearly as a function of the loading time from 0 to 0.6 degrees. The moment reaction caused by the rotation and the plastic strain of the beam are measured as functions of time. The moment reactions at different heating times are plotted as functions of rotation.

4.3 Finite elements and meshing

Ideally the beams would have been modelled using BEAM188 or BEAM189 elements in ANSYS Workbench, since they are based on the Timoshenko beam theory, which considers the shear deformation of the beam, and would be useful for the shear resistance portion of this study [6][7]. However, the convection and radiation boundary conditions do not support line body geometries [8][26]. BEAM elements are line elements, so they cannot be used [6][7]. For this reason, the beams must be modelled using SOLID elements. The thermal analysis is done using thermal solids. They are then replaced with structural solids for the structural analyses at different heating times. There are some curved surfaces in the model, but their curvature radius is large compared to the size of the elements on those surfaces. Therefore, it can be assumed that linear elements can

adequately approximate the surfaces, and quadratic elements are not needed. The geometries of the beams are suitable for sweeping and so prism and hexahedral elements should be used. Thus, SOLID70 elements are chosen for the thermal analysis and SOLID185 elements for the structural analysis. Thermal analysis also utilizes surface elements called SURF152.

SOLID70 is a linear three-dimensional thermal element. It has eight nodes, each with temperature as their only degree of freedom. In addition to a hexahedral element shape, the nodes at the element corners can be combined to form prism-, tetrahedron- or pyramid-shaped elements. The element can be used in both steady-state and transient thermal analyses. Orthotropic material properties are allowed. Convection, heat flux and radiation can be added as surface loads, although convection and heat flux cannot be applied at the same time. Heat generation rates can be added as body loads. There is also an option for mass transport available. All surfaces that are not next to another element and have no boundary constraints applied to them are assumed to be adiabatic. [35]

SURF152 is a thermal surface element. It can be placed on a face of any three-dimensional thermal element. The element can have either four nodes at the corners of the surface, or four at the corners and another four midside nodes. The surface nodes must match the nodes of the solid element the surface is placed on. Two additional nodes above the plane of the base element are possible in both cases. They can be used to better capture convection and radiation effects. A triangle-shaped element is possible. A thickness can be added to the element at the nodes. Radiation between the surface and the extra node is allowed. Convections and heat fluxes can be applied as surface loads and heat generation as a body load on the element. Each node has temperature as their single degree of freedom. [38]

SOLID185 is a linear three-dimensional structural solid with eight nodes. Each node has translations in x-, y- and z-directions as their three degrees of freedom. As for SOLID70, by combining the nodes of hexahedral elements, prism-, tetrahedron- and pyramid-shaped elements can be created. The element includes plasticity, hyperelasticity, stress stiffening and creep as well as large deflection and strain capabilities. SOLID185 can be used either as a homogeneous structural solid or as a layered structural solid for modelling layered thick solids or shells. The elements used in this study were homogeneous structural solids. This version of the element allows for orthotropic material properties. Pressures can be applied on the element faces as surface loads. Temperatures and body force densities can be input as body loads. [36]

The element size of the mesh was chosen using a sensitivity analysis. This study contains almost 300 calculations, so the calculation time should be as short as possible. The sensitivity analysis was done on a fully protected 200 mm long IPE 200-beam with five different element sizes, 5 mm, 4 mm, 3 mm, 2 mm and 1 mm. The result calculated using

the different mesh sizes and then compared was the bending moment reaction at the supported end of the beam in the middle of the fire (heating time 1800 s). The differences between consequent element sizes are shown in Figure 13.

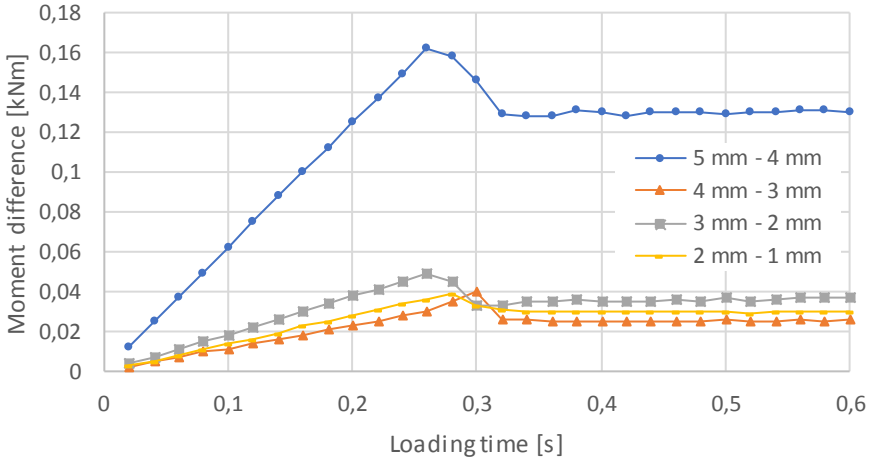

Figure 13. *The differences in bending moment reaction at the supported end of the beam between meshes of different element size as a function of loading time*

As can be seen, the differences in results between the mesh with an element size of 5 mm and a mesh with an element size of 4 mm are quite large, the maximum difference being 0.162 kNm at 0.26 s of loading time. The differences between 4 mm and 3 mm meshes, 3 mm and 2 mm meshes, as well as 2 mm and 1 mm meshes were significantly lower. It should also be considered that with the 1 mm mesh the calculation lasted for almost an hour. To minimize both the error caused by the choice of element size and the calculation time the element size was chosen to be 4 mm. Due to the similarities in shape between the cross sections studied, the same element size is used for both the IPE and HEA profiles. The meshes for fully protected IPE and HEA beams are shown in Figure 14 and Figure 15.

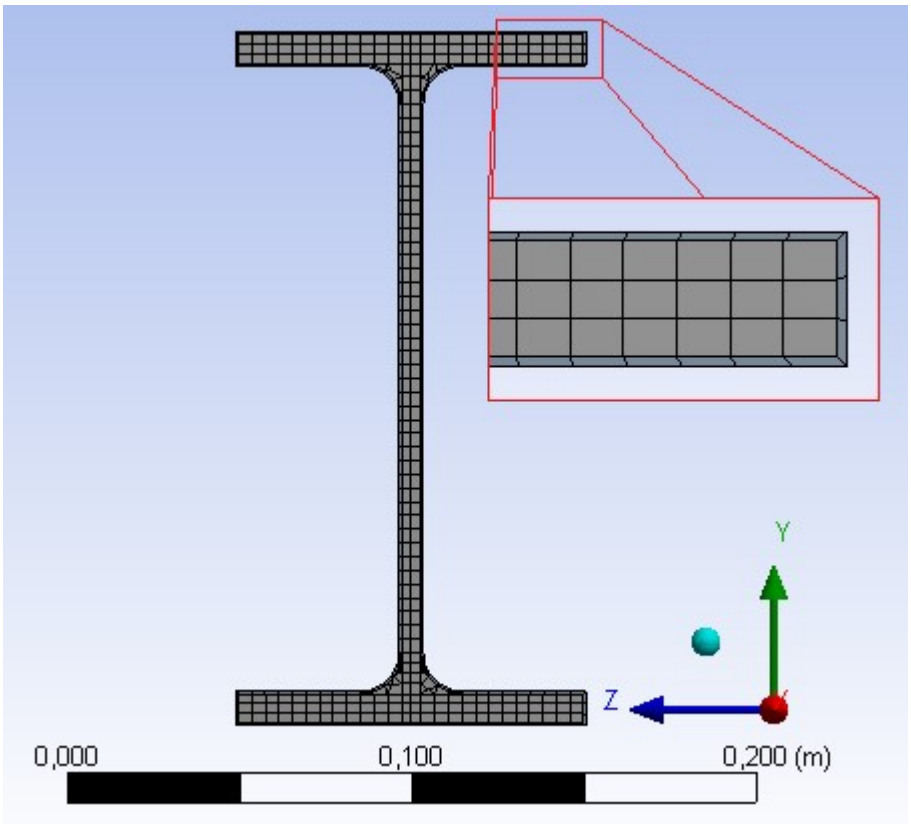

Figure 14. *The mesh used for IPE 200 [3]*

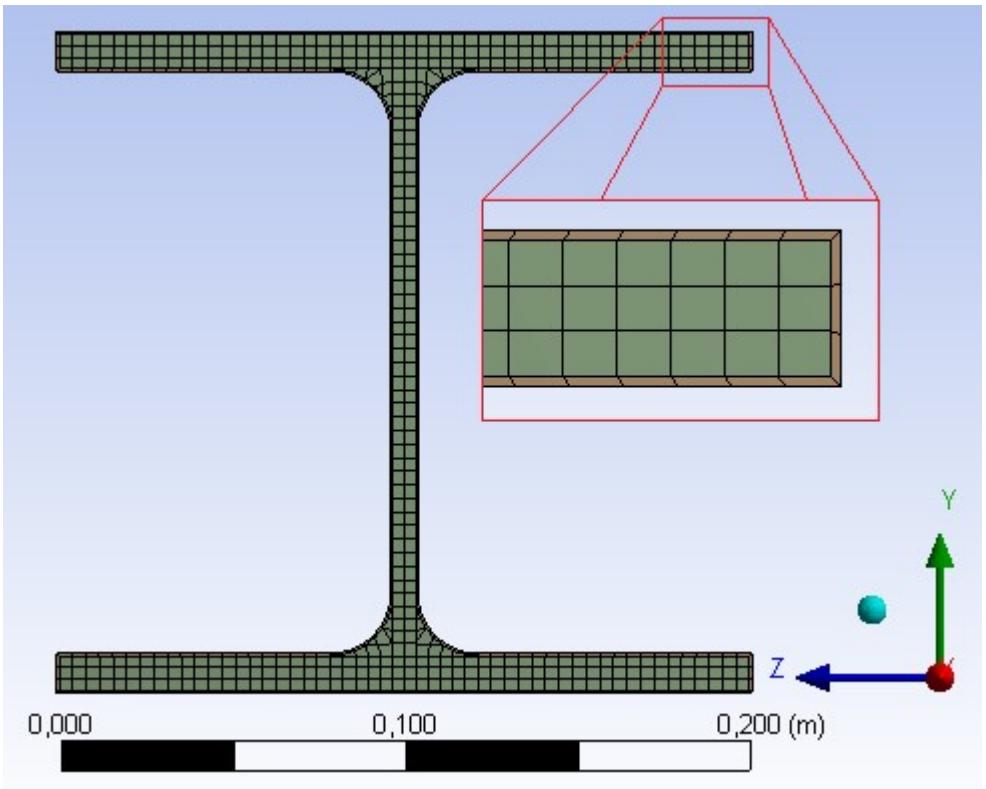

Figure 15. *The mesh used for HEA 200 [3]*

Since all the thermal and structural loads are uniform on the length of the beam, the elements were made to be the length of the beam as well. This was done to speed the calculations.

4.4 Validation of the model

The model was validated using test data from Tabeling [39] and data from Schaumann et al. [28]. Schaumann at al. modelled the conductivity of the intumescent coating by using the equivalent thermal conductivity and simulating the expansion of the coating. Both temperature curves are shown in the following graph (Figure 16), as well as the temperatures of the ISO-834 standard fire and the furnace temperature from the tests done by Tabeling. They are then compared to the data from the present study. The beam temperatures were calculated using both the standard fire and the furnace fire temperatures. All the beam temperatures were measured in the middle of the web of a fully protected IPE 200 beam.

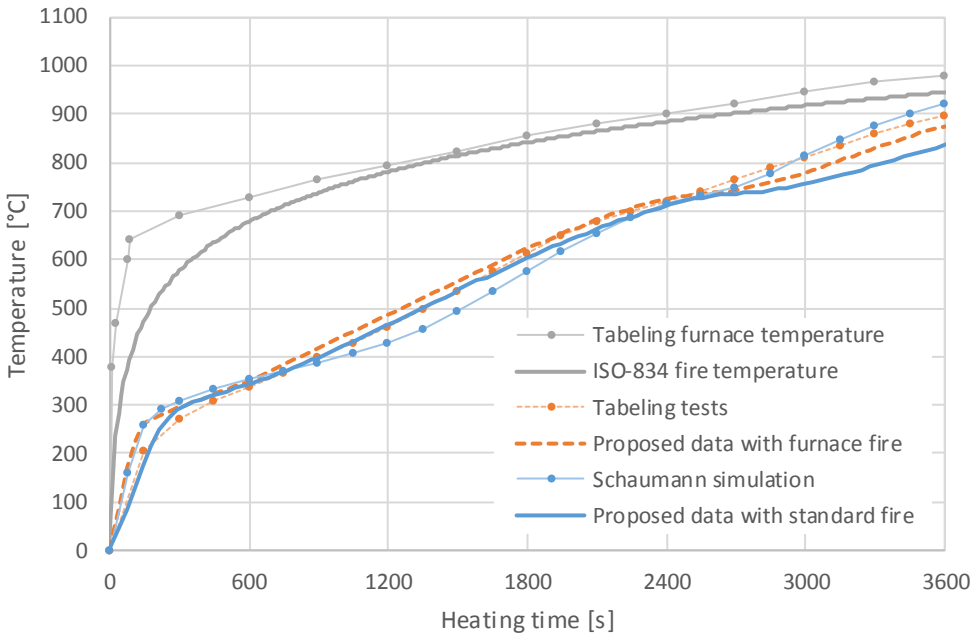

Figure 16. *The proposed temperature data from this study compared to data from a simulation and a test from previous research*

When comparing the data from the present study calculated using the standard fire to the data from the simulation by Schaumann et al. [28], it can be seen that the results match rather well. Between approximately 750 – 2250 s the model used in this study overestimates the model by Schaumann et al. by a maximum of 43.7 °C. The temperatures predicted by the model of this study are below the temperatures from Schaumann et al.'s model both under 750 s and above 2250 s, the maximum temperature differences being 78.4 °C and 88.3 °C respectively.

The temperatures from the tests by Tabeling [39] and the proposed model with the furnace fire are a better match. The temperatures from the model in this study are higher until around 2400 s, with the maximum difference being 57.8 °C. In the beginning of the fire the difference in temperatures is higher than later on in the middle parts of the fire, where the curves are very close to each other. After 2400 s the temperatures from the tests are higher, and the maximum difference is 32.3 °C.

From around 600 s to 2550 s the temperatures from the tests by Tabeling [39] and the model in this study with the standard fire are very close, the differences in temperature being between 0 – 15 °C. Before 600 s the maximum difference is 23.8 °C. After 2550 s the differences in temperatures start to grow, with the maximum being 64.4 °C. However, the used model with standard fire corresponds well with the results from the tests by Tabeling.

As can be seen the above curves for a fully protected IPE 200 beam are close, therefore the results can be assumed to validate the IPE 200 models of this study. The following Figure 17 shows the temperatures in the middle of the web for both fully protected IPE 200 and HEA 200 beams as a function of time.

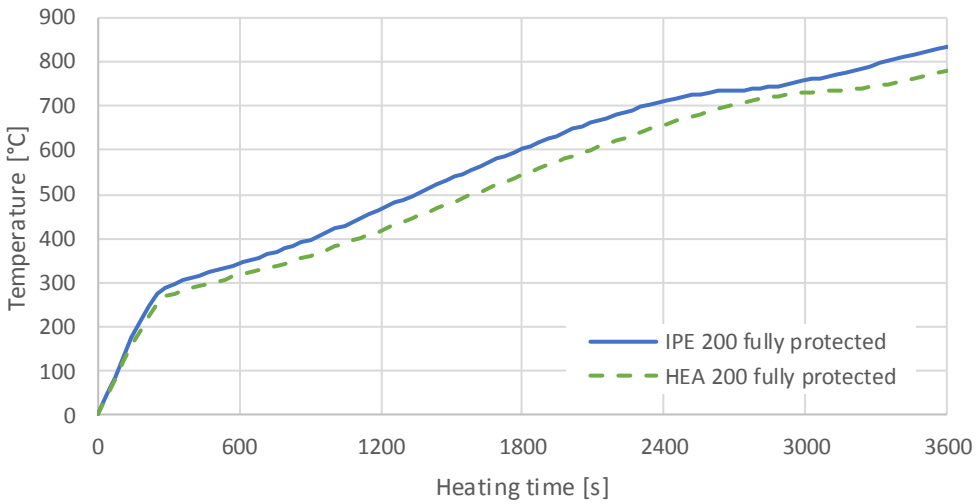

Figure 17. *Comparison of calculated temperatures for fully protected IPE 200 and HEA 200 beams*

The shapes of the curves are very similar. The IPE 200 beam reaches higher temperatures slightly faster, but the results are still very much alike. The small differences in shape for the two profiles don't seem to affect the temperature curve significantly. Therefore, it can be assumed that the HEA 200 model is also validated, since the data from the Schaumann et al.'s model [28] and the test data by Tabeling [39] validate the IPE 200 model.

5. RESULTS

5.1 Temperatures

As mentioned before, thermal analyses are done for both types of beams, for all three types of loading cases and for all three levels of fire protection. Since the beam length is the same when calculating bending and torsion resistance, the thermal analysis is also the same. The following sets of temperature curves shown in Figure 18 and Figure 19 show the beam temperatures for both profiles. Each set shows the temperature of the beam at four different locations on the cross section as a function of time for the different fire protection levels.

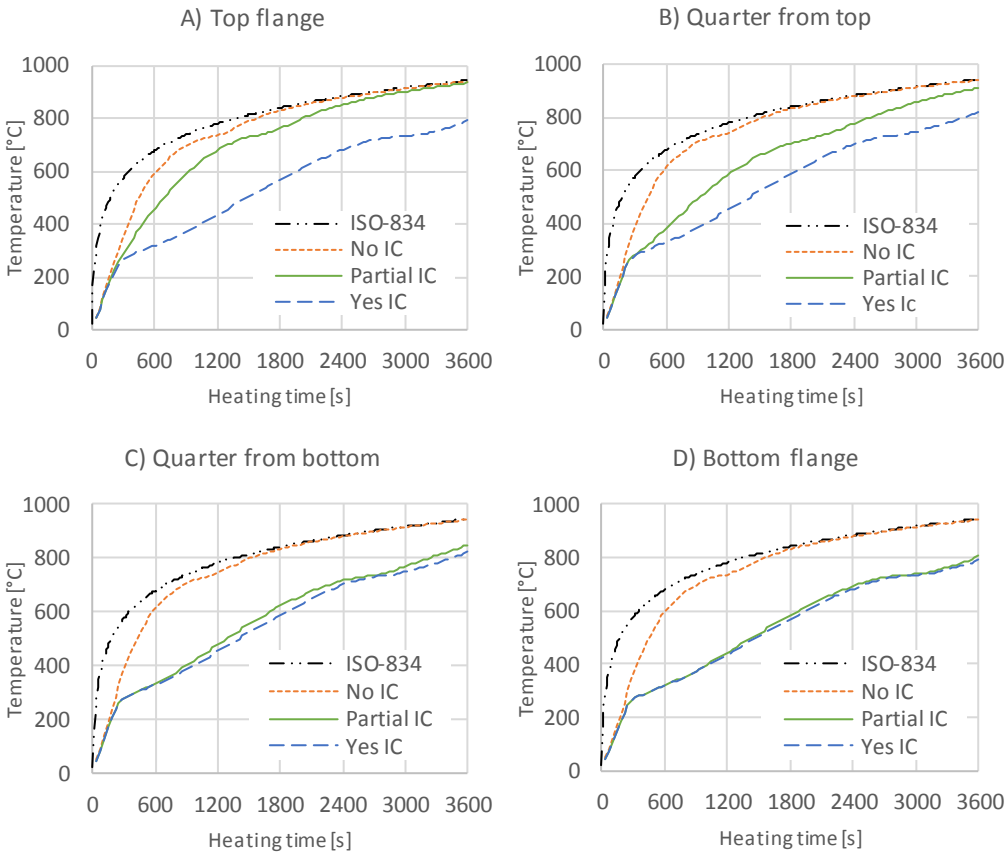

Figure 18. *The temperature curves of the ISO-834 fire and the IPE 200 beam for all levels of fire protection at different points (A-D) on the cross section*

The above graphs show the temperature curve of the fire and the temperature of the IPE 200 beam at points which are on the outer surface of the top flange (A), a quarter of the beam's height from the top (B), a quarter of the beam's height from the bottom (C) and the outer surface of the bottom flange (D). Each graph shows a temperature curve for when the beam is fully covered with intumescent coating, when it is not coated and when

it is partially coated. It can be seen that the curves for the fully coated beam do not significantly differ from each other at different locations, nor do the curves for the unprotected beam. However, the curve for the partially protected beam changes quite considerably with the location. At point A the temperatures of the partially protected and unprotected beam are very close together. When moving from point A towards point D, the temperature curve of the partially protected beam starts to move closer to the curve of the fully protected beam. It should be noted that the intumescent coating on the other surfaces of the profile has a bigger effect on the temperature of the partially protected beam than the unprotected top flange does. This can be seen in the way that the temperature curves of the partially and fully protected beams are almost identical at point D, whereas the curves for the unprotected and partially protected beams are slightly different at point A. Even the curves of the partially protected beam at points B and C show this, since the curves tend to be closer to the fully protected beam's curve.

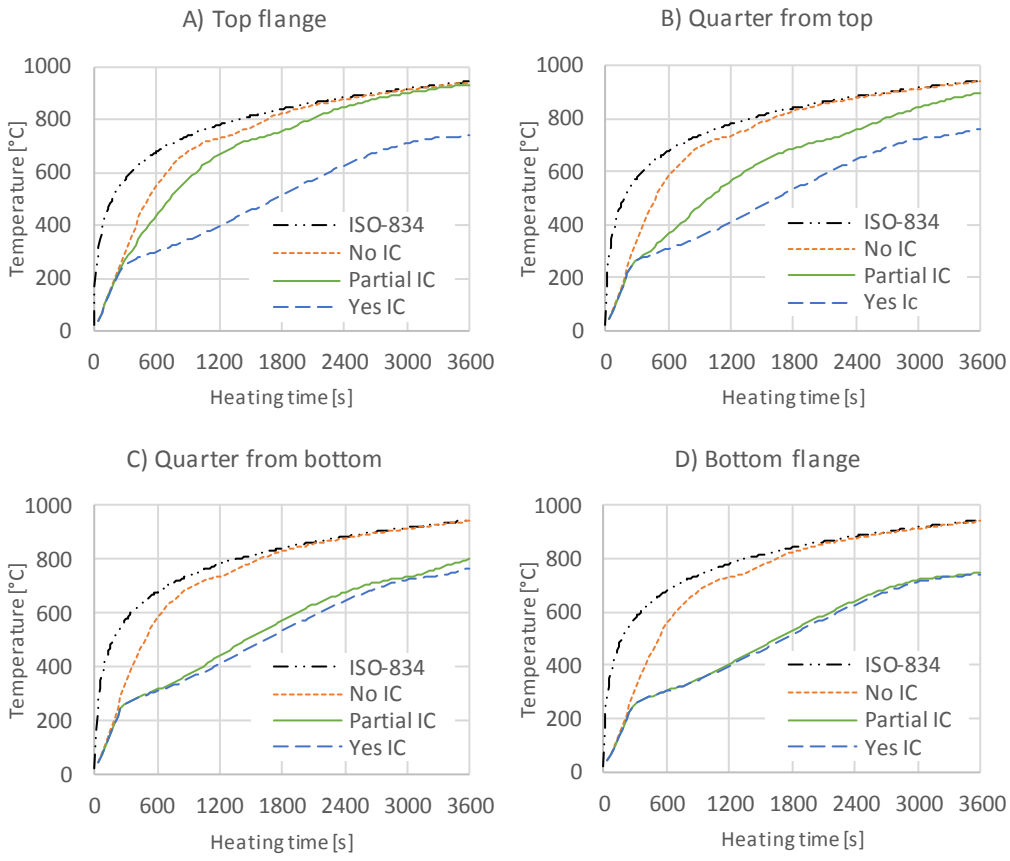

Figure 19. *The temperature curves of the ISO-834 fire and the HEA 200 beam for all levels of fire protection at different points (A-D) on the cross section*

As can be observed, the temperature curves for IPE 200 and HEA 200 beams shown in Figure 18 and Figure 19 are very much alike. The curve of the partially protected HEA 200 beam behaves similarly when moving from the top flange (A) towards the bottom flange (B) as it did for IPE 200. There are some minor differences between the curves of the two beams, mainly that the IPE 200 beam reaches high temperatures slightly faster,

especially when comparing the curves of the fully protected beams (see Figure 18). This is likely due to the ratio of the cross-sectional area to the perimeter of the HEA 200 profile being bigger. Thus, the HEA 200 beam has relatively less surface area covered with intumescent coating for heat to move through to heat up a larger volume of steel than the IPE 200 profile does. When the beams are unprotected, the temperature curves are approximately the same, so the difference in the dimensions have a negligible effect on the temperature curves. This can be seen in Figure 20.

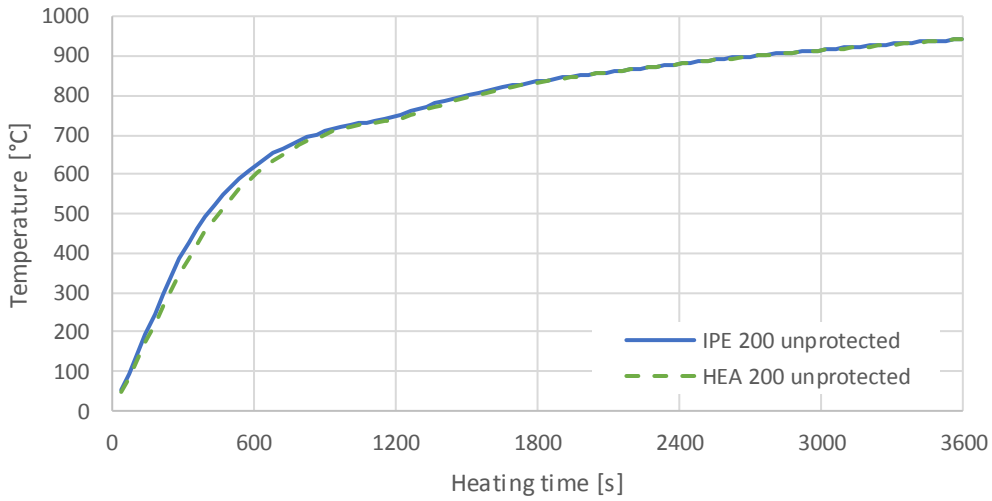

Figure 20. *Comparison of calculated temperatures for unprotected IPE 200 and HEA 200 beams*

The temperatures discussed so far were calculated from the models used to find the bending and torsion resistances, where the beam was 200 mm long. In the shear resistance models the beam is 10 mm long. The temperatures at different measuring points differ very little between the two lengths. The maximum difference in temperatures at different measuring points for IPE 200 varies between 0.0 - 0.22 °C and for HEA 200 they vary between 0.0 - 1.35 °C. Therefore, the temperature curves presented can be assumed to apply in the case of both beam lengths.

The temperature gradients shown in Figures 18 and 19 affect the yield strengths of the beams, as mentioned before. The yield strength distributions of a partially protected IPE 200 beam for four different heating times are shown in Figure 21.

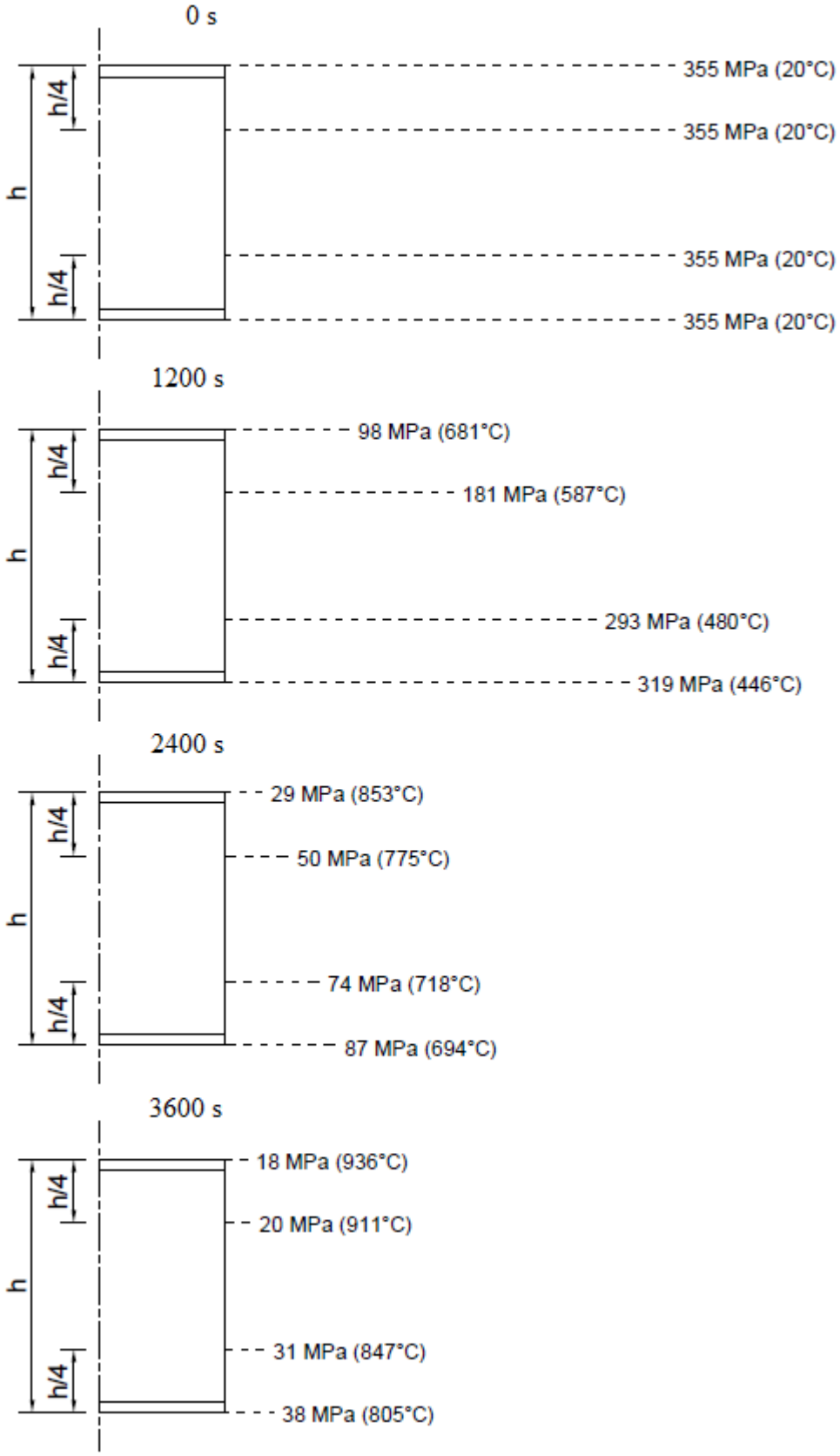

Figure 21. *The yield strength in different points of a profile at different heating times*

The beams are viewed from the side. The upper flange is unprotected, while all the other sides are fully protected with intumescent coating. The yield strength is given on the outer surface of both flanges, as well as in points that are one quarter of the beam's height (h) from the top and the bottom. The temperatures shown are from the temperature results of the IPE 200 models (see Figure 18), and the yield strengths are determined according to the material model of steel (see Figure 8). The lengths of the dotted lines indicate the yield strength in different measuring points at the indicated times.

As can be seen, the non-uniform heating of the beam causes an uneven yield strength distribution on the beam profile, especially in the middle of the fire. After 20 minutes (1200 s) of heating the temperature of the upper flange is already so high that the yield strength of the steel is under a third of the strength in room temperature. However, the bottom flange has still retained most of its strength. After 40 minutes (2400 s) this is no longer the case. The temperature of the bottom flange has increased enough so that the yield strength has fallen to about one fourth of the original value, and the strength of the steel on the top flange is only about one tenth of the original yield strength. Finally, after 60 minutes (3600 s) the yield strength distribution has levelled so, that it is rather even over the cross section. The temperatures are high enough that the strength values are one tenth of the original strength values at the lower parts of the profile and under that at the upper parts.

As a comparison, when the profile is either fully protected or unprotected the temperature changes are very even throughout the whole cross section. This can be seen from the temperature results of the IPE 200 models (Figure 18). The temperatures at the bottom flange (D) of the partially protected profile are approximately the same as the temperatures of the fully protected profile in all measuring points. The temperatures at the upper flange (A) of the partially protected beam are slightly lower than the temperatures of the unprotected beam in all measuring points. Therefore, at all four heating times the yield strength of the entire cross section of a fully protected beam is approximately the same as the yield strength values of the partially protected beam on the bottom flange, and for an unprotected beam the yield strength is slightly lower than the values of a partially protected beam at the top flange.

5.2 Bending resistance

As mentioned before, the moment reaction at the support is plotted as a function of rotation for all heating times. Figures 22, 23 and 24 show the rotation-moment curves for an IPE 200 beam when it is fully protected, partially protected and unprotected.

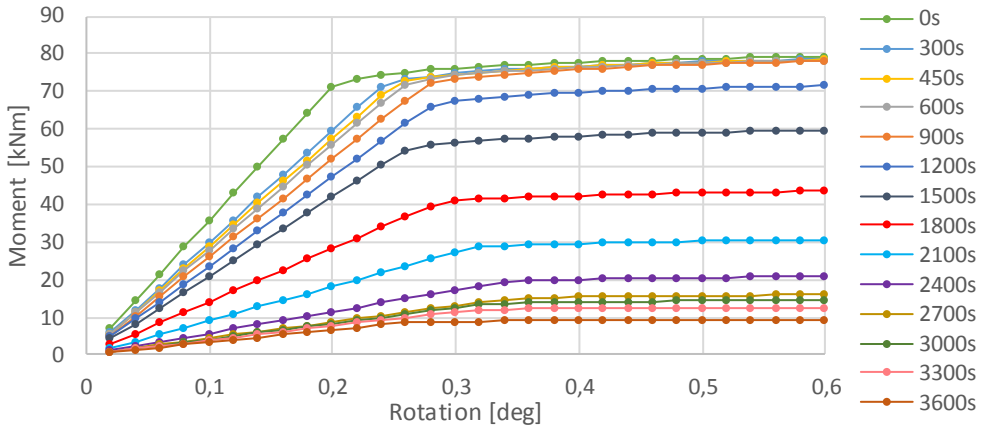

Figure 22. *Rotation-moment curves for bending for the fully protected IPE 200 beam*

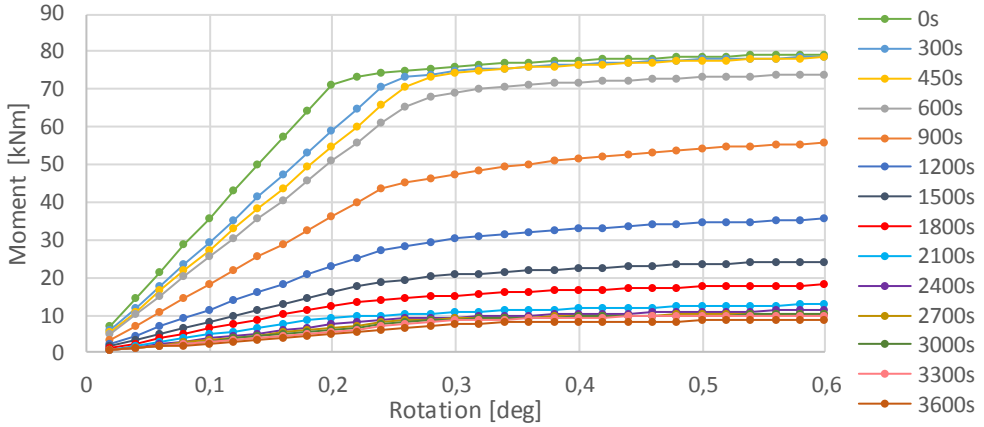

Figure 23. *Rotation-moment curves for bending for the partially protected IPE 200 beam*

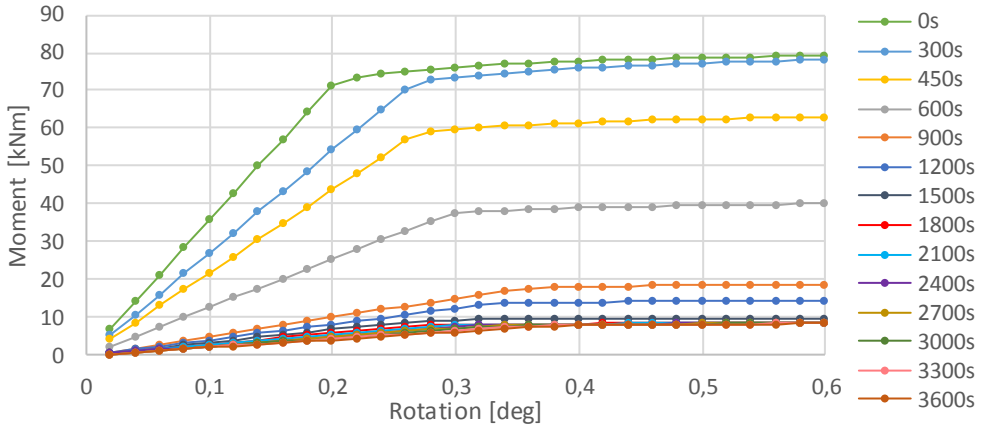

Figure 24. *Rotation-moment curves for bending for the unprotected IPE 200 beam*

The moment increases linearly with rotation until the beam reaches its bending resistance and the curve turns almost horizontal. The ends of the curves are not fully horizontal due to the linear elastic, linear strain hardening material model. The exact bending resistance

is read from the curve at the rotation when the plastic strain of the beam reaches 0.2 %. The curves show how the strength of the steel decreases as its temperature rises. The higher the heating time the earlier the curve turns horizontal. The insulating effect of the intumescent coating can also be seen on the locations of the curves. For the unprotected beam most of the curves are on the lower part of the graph, close to 10 kNm, whereas for the fully protected beam the high temperatures of the fire take longer to lower the bending resistance and the curves are more evenly distributed on the plot. The effects of heating times and different levels of fire protection are visible for all rotation-moment and displacement-force curves in future chapters as well.

This thesis was based on the work of Hautala et al. [17]. The following Figure 25 shows both the results from Hautala et al. for the bending resistance of an IPE 200 beam, and the bending resistance results for the same beam obtained in this study.

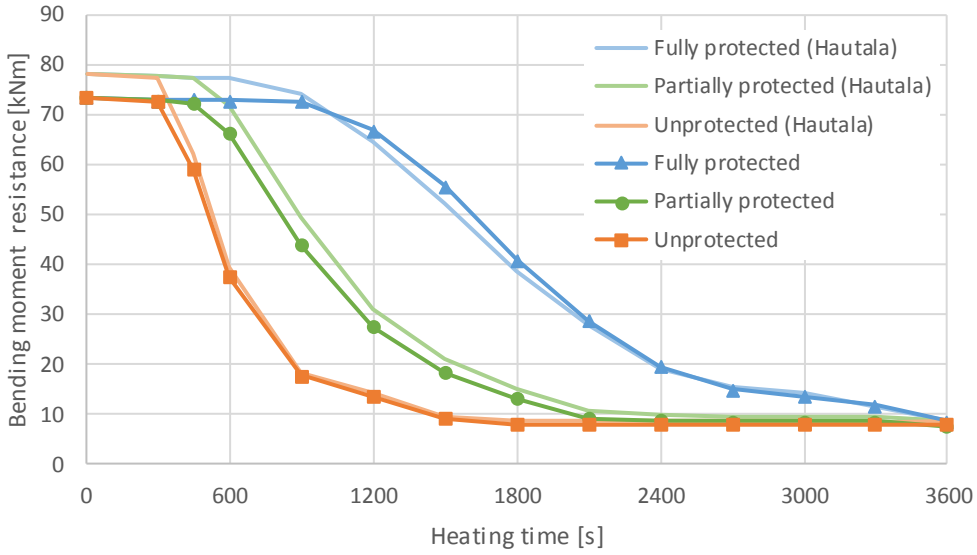

Figure 25. *Bending moment resistance of the IPE 200 beam for three levels of fire protection*

The results of this study vary slightly from the results by Hautala et al., but the shapes of the curves are similar. The insulating effect of the intumescent coating on the partially protected beam is most visible in the middle of the fire, between 300 s and 2100 s (5 – 35 minutes). Before and after this period of time the bending resistances of the partially protected and unprotected beam are nearly the same. The bending resistance of the fully protected beam falls to half of its original value in about 31.7 minutes (1903 s). The partially protected beam reaches this value in 17.2 minutes (1033 s), and the unprotected beam's resistance halves in 10.2 minutes (614 s).

The rotation-moment curves for all three levels of fire protection are plotted for the HEA 200 beam as well. They are shown in Figures 26, 27 and 28.

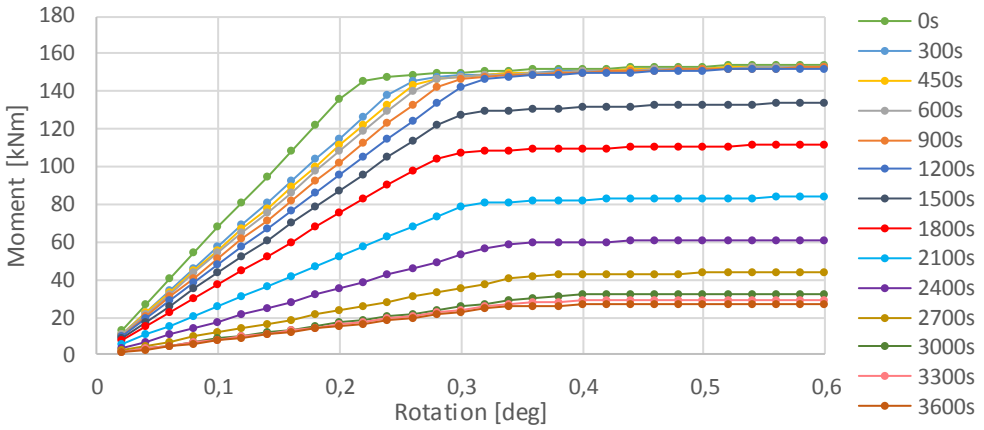

Figure 26. *Rotation-moment curves for bending for the fully protected HEA 200 beam*

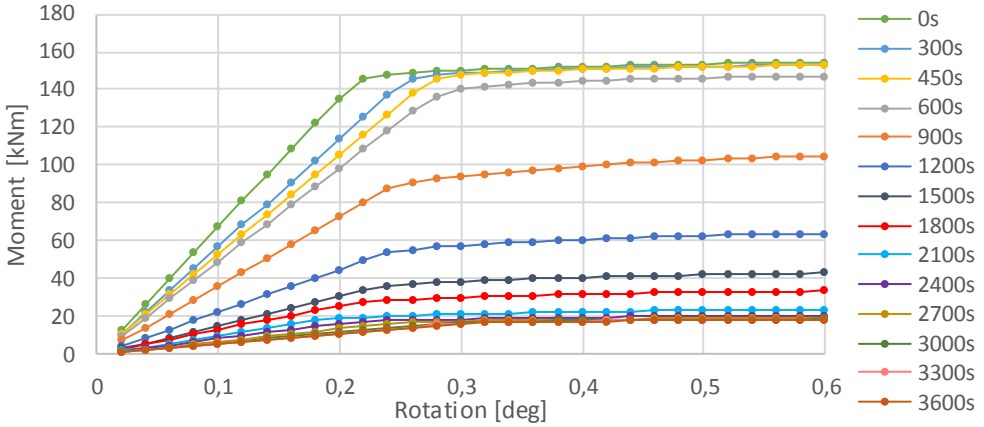

Figure 27. *Rotation-moment curves for bending for the partially protected HEA 200 beam*

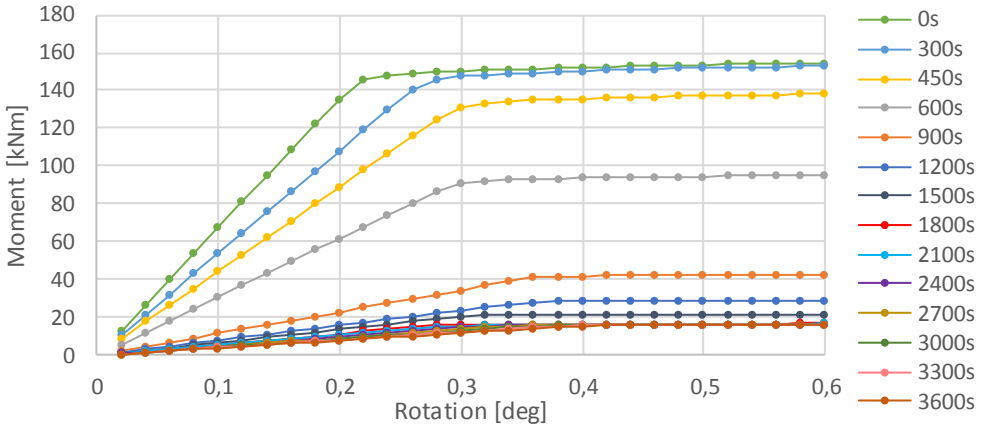

Figure 28. *Rotation-moment curves for bending for the unprotected HEA 200 beam*

These curves are similar to the ones for the IPE 200 beam. The moment reaction at the support rises linearly until the beam reaches its bending resistance and the curve turns

nearly horizontal. The bending resistances on the resistance curves are read from the rotation-moment plots when the plastic strain reaches 0.2 %. They are shown in Figure 29.

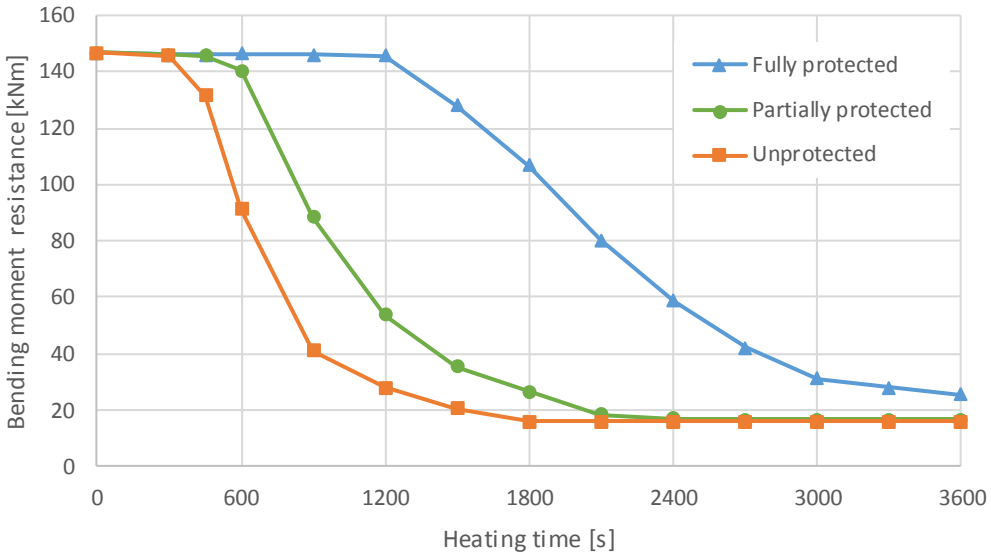

Figure 29. *Bending moment resistance of the HEA 200 beam for three levels of fire protection*

The intumescent coating has the largest effect on the resistance between 5 and 35 minutes (300 s – 2100 s) as earlier. The fully protected beam's resistance is halved in 36.6 minutes (2197 s), the partially protected beam's half time is 17.2 minutes (1031 s), and the unprotected beam's resistance is halved in 11.8 minutes (707 s).

There is some variance in the half times of the beams' resistances. They are shown in Table 2.

Table 2. *The half times of the bending resistances for IPE 200 and HEA 200*

Fire protection	IPE 200 half times	HEA 200 half times	Differences in half times
	min	min	min
Fully protected	31.7	36.6	4.9
Partially protected	17.2	17.2	0.0
Unprotected	10.2	11.8	1.6

It takes 4.9 minutes longer for the fully protected HEA 200 beam's resistance to fall to half of its original value compared to the fully protected IPE 200 beam. This is due to the IPE 200 beam reaching higher temperatures faster, as mentioned before.

Bending is mostly carried by the flanges of the profiles. The flanges of the HEA 200 profile are wider than those of the IPE 200 profile, so its unprotected area is also larger. Moving from full fire protection to partial protected increases the speed at which the temperature of the beam rises. The larger unprotected area of the HEA 200 beam causes the

increase in heating speed to be larger than for the IPE 200 beam. For this reason, the half time of the HEA 200 beam drops more than that of the IPE 200 beam when moving from full protection to partial protection.

5.3 Shear resistance

The displacement-force curves are plotted for all heating times and all three levels of fire protection. They are shown in Figures 30, 31 and 32 for an IPE 200 beam.

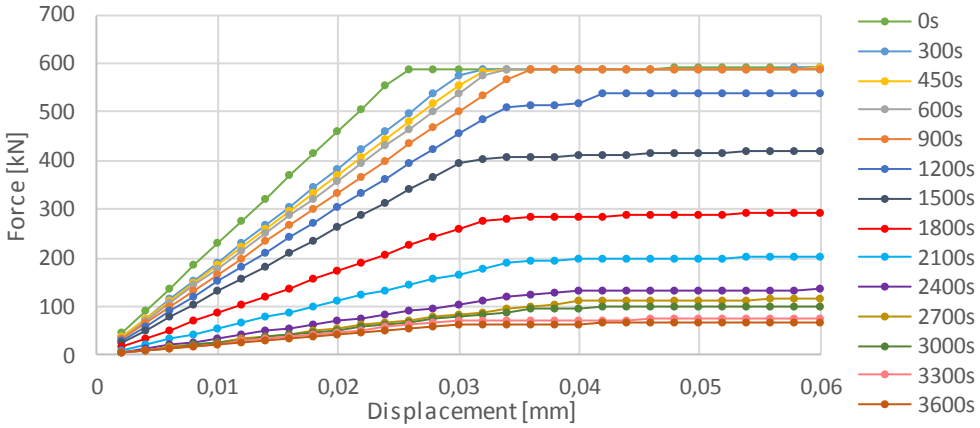

Figure 30. *Displacement-force curves for the fully protected IPE 200 beam*

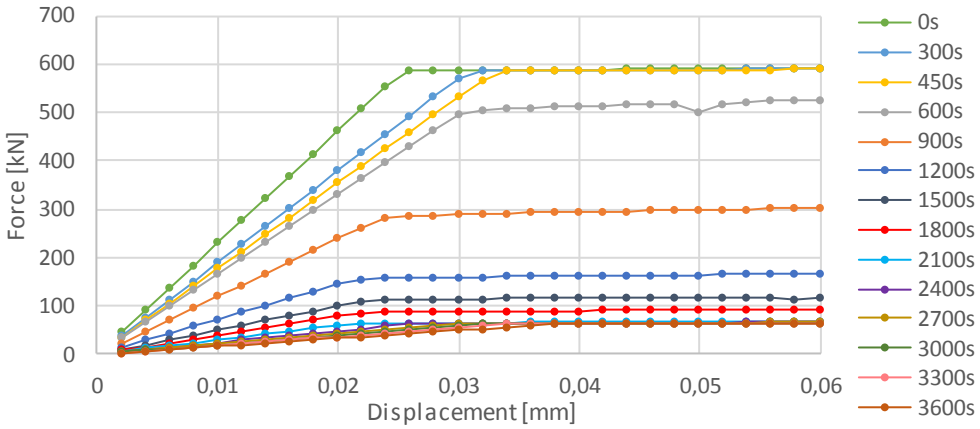

Figure 31. *Displacement-force curves for the partially protected IPE 200 beam*

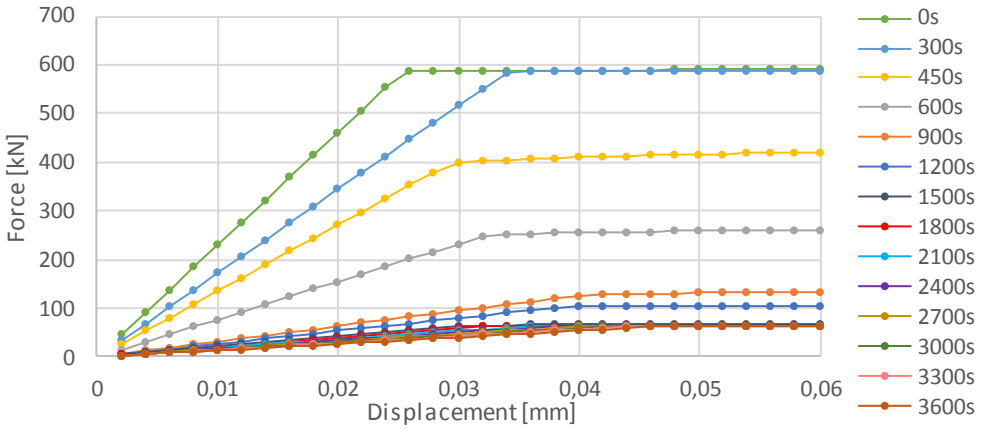

Figure 32. *Displacement-force curves for the unprotected IPE 200 beam*

The displacement-force curves are generally similar in shape to the rotation-moment curves. There is some mild unevenness on the curves, likely due to the unconventional beam length. The irregularity is so small, however, that it can be assumed to be negligible. The shear resistance values are read from the curves when the plastic strain of the beam's web has reached 0.2 % and are shown in Figure 33 for the different levels of fire protection.

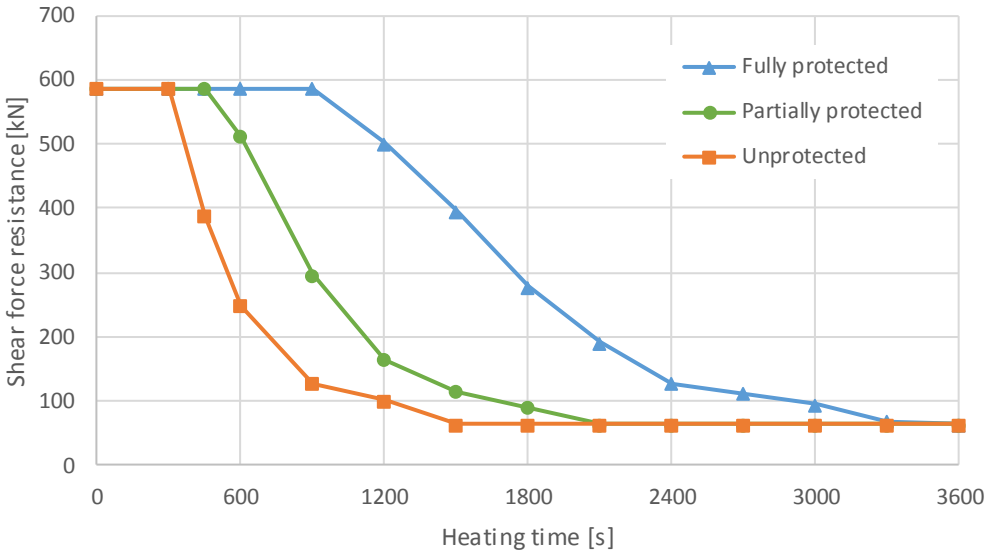

Figure 33. *Shear force resistance of the IPE 200 beam for three levels of fire protection*

The added fire protection affects the shear resistance of the beam mostly between times 5 and 35 minutes compared to the unprotected beam. It takes 29.3 minutes (1760 s) for the fully protected beam's shear resistance to be halved, 15.1 minutes (907 s) for the partially protected beam's resistance, and 9.2 minutes (552 s) for the unprotected beam's resistance.

Next, the displacement-force plots for the HEA 200 beam are shown. The graphs are shown in Figures 34, 35 and 36.

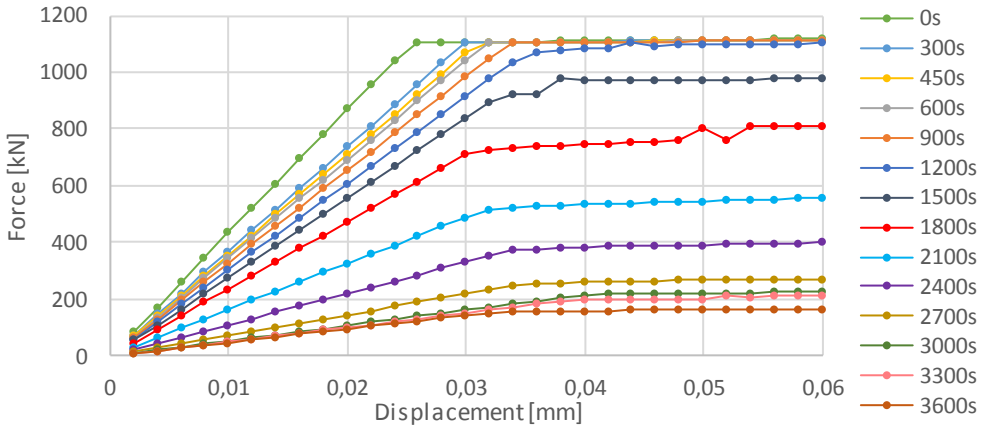

Figure 34. *Displacement-force curves for the fully protected HEA 200 beam*

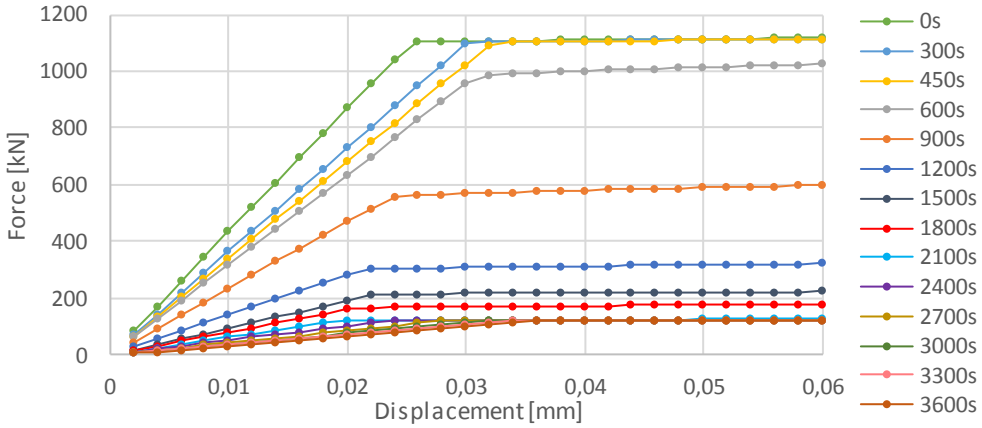

Figure 35. *Displacement-force curves for the partially protected HEA 200 beam*

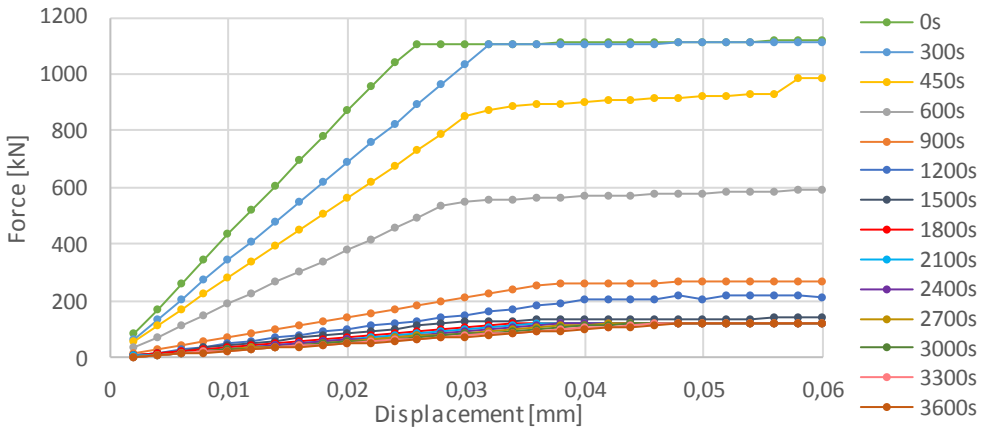

Figure 36. *Displacement-force curves for the unprotected HEA 200 beam*

The shape of the curves is again similar to the IPE 200 beam's displacement-force curves. These curves also have some negligible irregularities. The graphs are used to plot the

shear force resistance curves as a function of the heating time for the three cases of fire protection. The resistances are read from the curves when the plastic strain of the web of the beam is 0.2 %. They are shown in Figure 37.

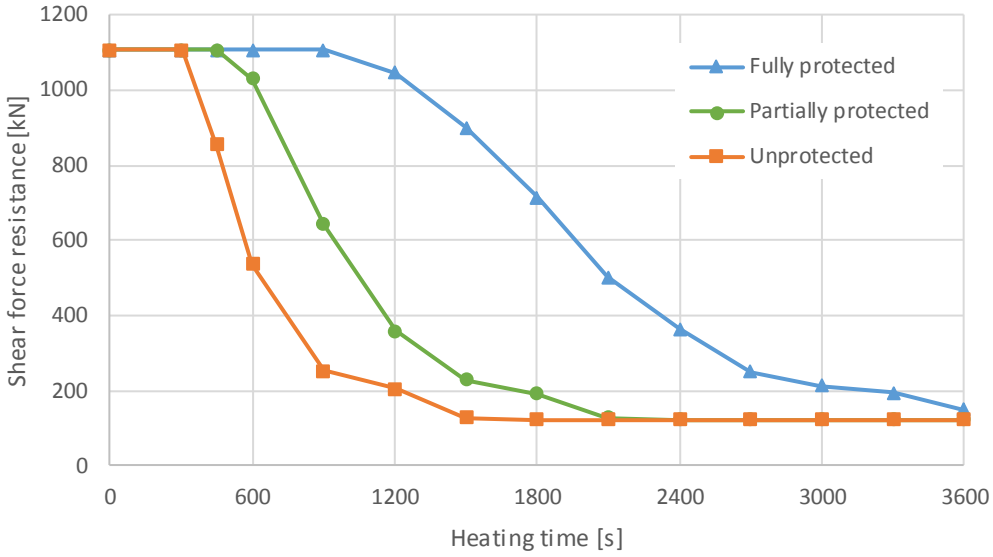

Figure 37. *Shear force resistance of the HEA 200 beam for three levels of fire protection*

The effect of the added intumescent coating of the partially protected beam is, as before, mostly visible between times 5 and 35 minutes. Before and after this time period the resistance curve of the partially protected beam follows the curve of the unprotected beam. The half time for the fully protected beam is 33.8 minutes (2028 s), for the partially protected beam it is 16.5 minutes (993 s), and for the unprotected beam it is 9.9 minutes (592 s).

There is again some deviation between the half times of the two beams. Table 3 shows the differences between the half times.

Table 3. *The half times of the shear resistances for IPE 200 and HEA 200*

Fire protection	IPE 200 half times	HEA 200 half times	Differences in half times
	min	min	min
Fully protected	29.3	33.8	4.5
Partially protected	15.1	16.5	1.4
Unprotected	9.2	9.9	0.7

As before, for the half times of the bending resistances, the difference in half times is quite large. This is caused by the IPE 200 beam heating up faster as mentioned earlier.

The half times of the partially protected beams were the same when the bending resistance was studied (see Table 2). Here, however, they are not. Shear force is mostly carried by

the web of the cross section. Since the web is farther away from the unprotected surface than the flange is, the effect of moving from full protection to partial protection is not quite as significant for shear as it was for bending. Still, the larger unprotected area of the HEA 200 beam does cause the difference in half times of the partially protected beams to decrease.

The temperature curves of the unprotected beams are nearly the same, as was shown before in Figure 20. This causes the half times of the unprotected beams to be nearly the same.

5.4 Torsion resistance

The rotation-moment curves for torsion are plotted. They are shown for the fully protected, partially protected and unprotected IPE 200 beams in Figures 38, 39 and 40.

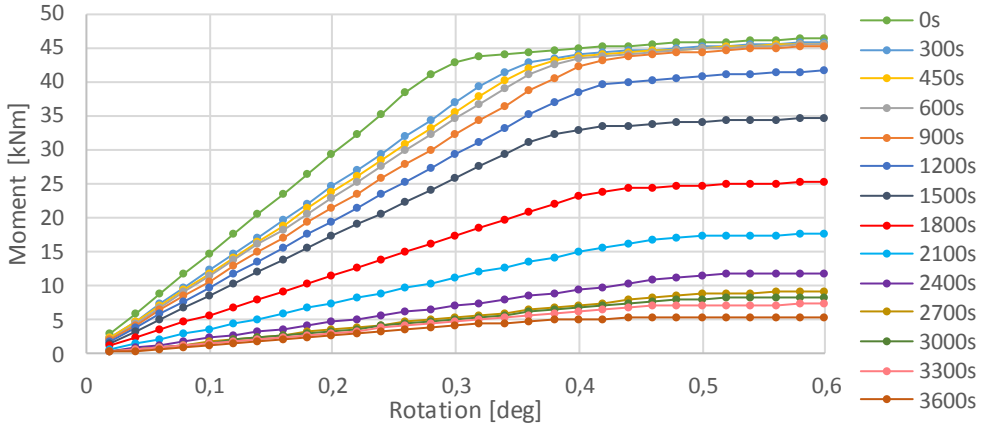

Figure 38. *Rotation-moment curves for torsion for the fully protected IPE 200 beam*

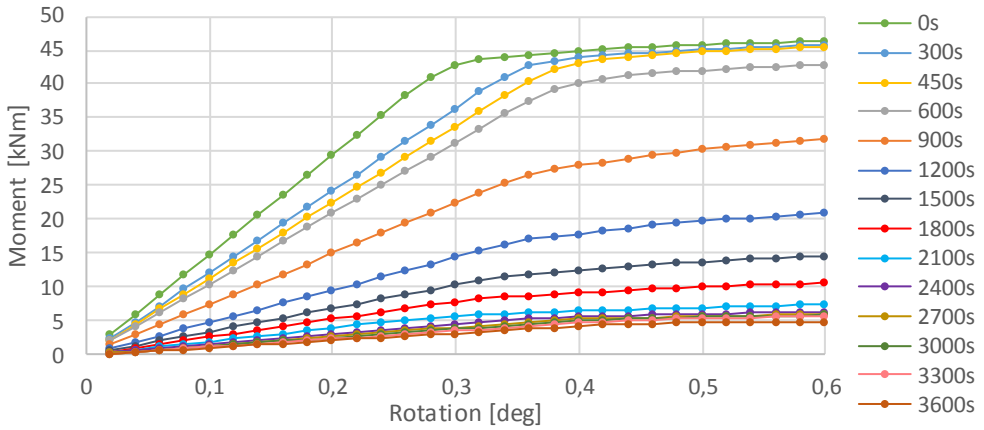

Figure 39. *Rotation-moment curves for torsion for the partially protected IPE 200 beam*

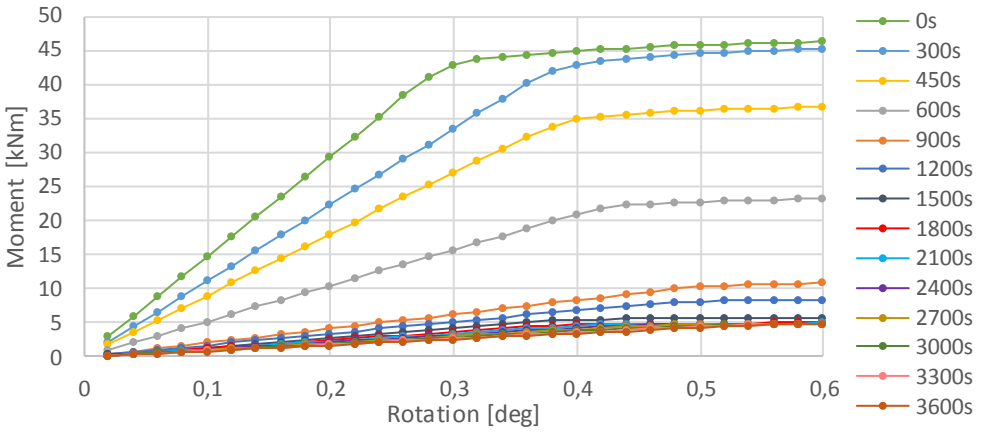

Figure 40. *Rotation-moment curves for torsion for the unprotected IPE 200 beam*

The curves are similar in shape to the earlier rotation-moment curves and the displacement-force curves, even though the bend where the beam reaches its resistance is much softer than in the earlier curves. The torsion resistances are measured from the plots when the plastic strain of the cross section reaches 0.2 %. Using these values, the heating time-torsion moment resistance graph is plotted. It is shown in Figure 41.

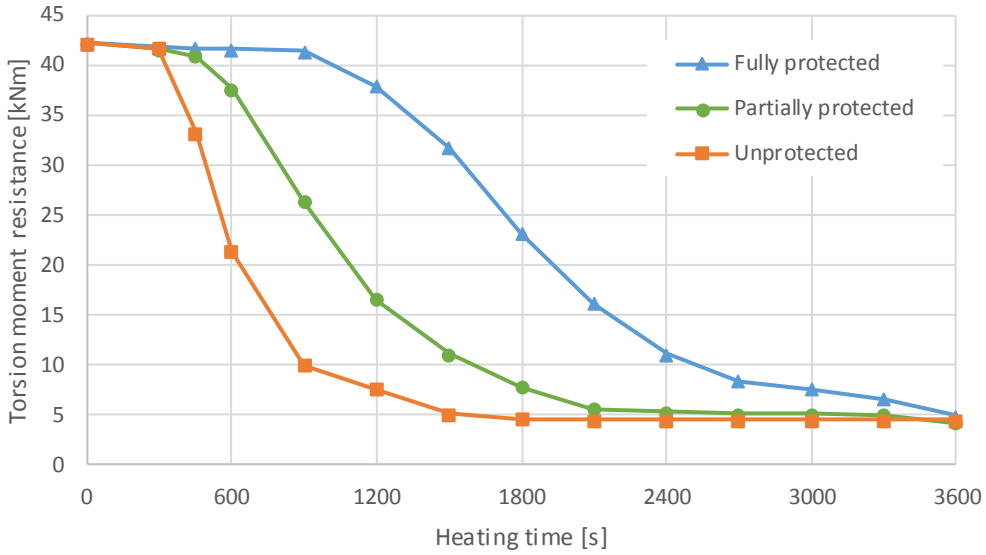

Figure 41. *Torsion moment resistance of the IPE 200 beam for three levels of fire protection*

The effect of the added thermal insulation of the partially protected beam can again be mostly seen between 5 and 35 minutes. The time it takes to halve the torsion resistance of the fully protected beam is 31.5 minutes (1889 s), for the partially protected beam's resistance it takes 17.7 minutes (1061 s), and for the unprotected beam it takes 10.1 minutes (608 s).

Lastly, the rotation-moment curves for the HEA 200 beam are plotted. They are shown in Figures 42, 43 and 44 for all levels of fire protection.

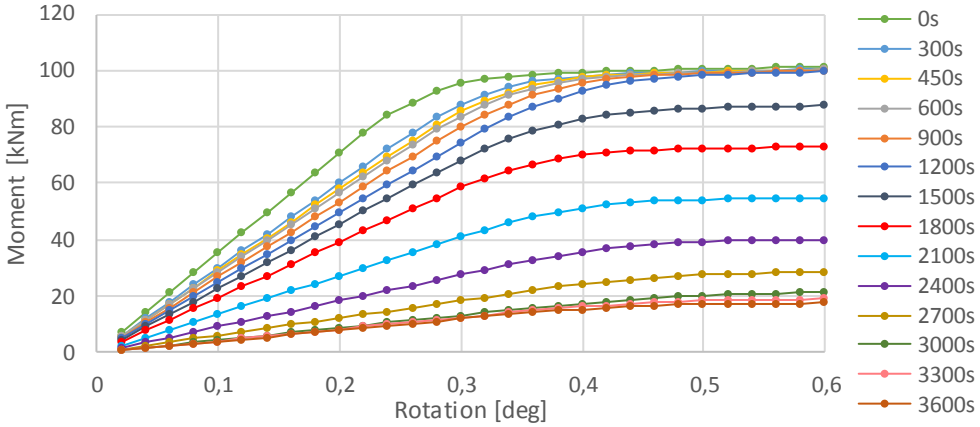

Figure 42. *Rotation-moment curves for torsion for the fully protected HEA 200 beam*

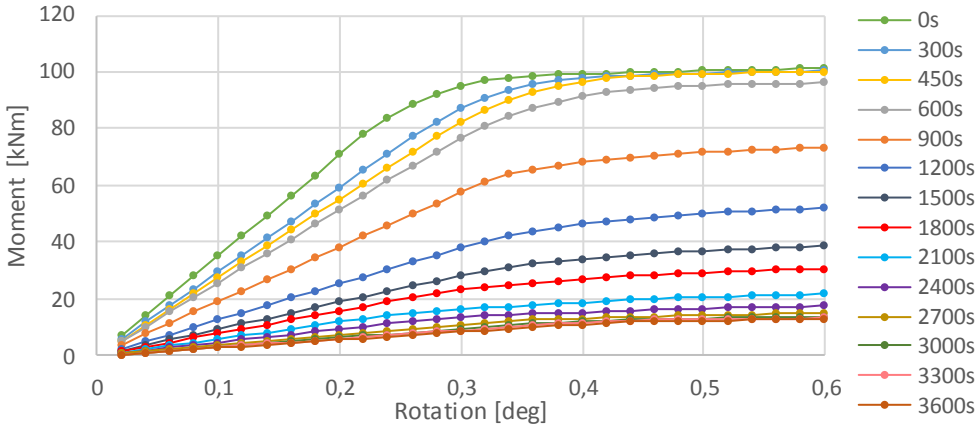

Figure 43. *Rotation-moment curves for torsion for the partially protected HEA 200 beam*

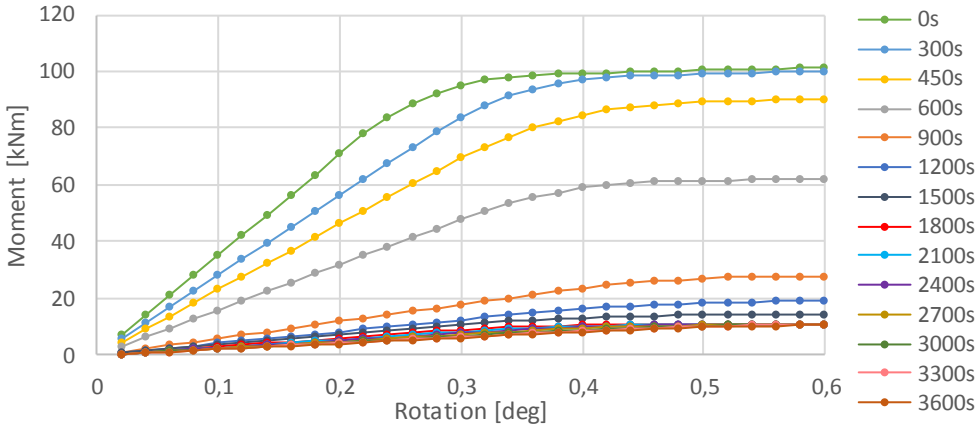

Figure 44. *Rotation-moment curves for torsion for the unprotected HEA 200 beam*

For these curves the bend, where the beam reaches its resistance is the softest so far. The general shape of the curves still remains the same. These curves are used to create the torsion moment resistance curves as a function of time seen in Figure 45. The torsion resistance values are read from the curves in Figures 42, 43 and 44 when the plastic strain of the cross section reaches 0.2 %.

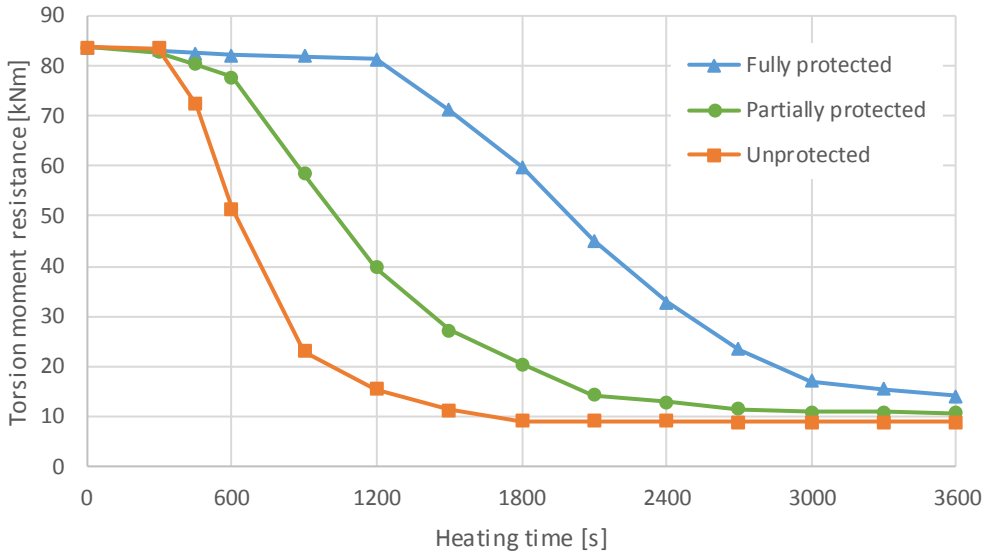

Figure 45. *Torsion moment resistance of the HEA 200 beam for three levels of fire protection*

Unlike for all the other heating time-resistance graphs shown in this study before, the effect of the additional intumescent coating of the partially protected beam can be seen between 5 and 45 minutes, even though during the time period between 35 and 45 minutes very little additional resistance is gained. The half time of the resistance of the fully protected beam is 36.3 minutes (2177 s), for the partially protected beam it is 19.4 minutes (1166 s) and for the unprotected beam 11.7 minutes (701 s).

There is again some variation between the half times of the two beams. The differences between the half times are shown in Table 4.

Table 4. *The half times of the torsion resistances for IPE 200 and HEA 200*

Fire protection	IPE 200 half times	HEA 200 half times	Differences in half times
	min	min	min
Fully protected	31.5	36.3	4.8
Partially protected	17.7	19.4	1.7
Unprotected	10.1	11.7	1.6

The difference between the half times of the fully protected beams is rather large. It seems, that the difference in half times of the fully protected beams does not significantly

depend on the loading case, at least not for the loading types and profiles studied in this thesis. For the cases in this study it has been 4.5 – 4.9 minutes for all loading types.

As before, the larger unprotected surface of the HEA 200 profile increases the speed at which the temperature of the beam rises more than the unprotected surface of the IPE 200 profile does. This shows in the difference between the half times falling from 4.8 minutes to 1.7 minutes when moving from full protection to partial protection. However, when comparing the partially protected and unprotected beams, the difference in half times stays approximately the same. When the partial protection is removed, the temperature gradient of the beam becomes more even over the cross section and the temperatures generally rise higher. Removing the intumescent coating from the top flange of the fully protected beam of course causes the temperature of the beam to rise, but after this it seems that the shape of the profile influences the torsion resistance of the beam more than the higher, more even temperature gradient of the unprotected beam does. The further away the points of the profile are from the center of twist the greater the value of the torsion modulus of the profile is. The outer corners of the HEA 200 profile are further away from its center of twist than those of the IPE 200 profile. This is because the dimensions of the HEA 200 beam (height 190 mm and width 200 mm) make it a more square-shaped profile than the IPE 200 beam (height 200 mm and width 100 mm). This causes the HEA 200 profile to have a greater torsion modulus, and therefore explains the difference in the half times staying constant after the intumescent coating on the outer surface of the top flange is removed.

As an added curiosity, the torsion model is shown at the start, middle and end of the fire, since the effect of the uneven temperature gradient can best be seen from the torsion model of the partially protected beam. The following Figure 46 shows plastic strain for the IPE 200 beam at three different heating times.

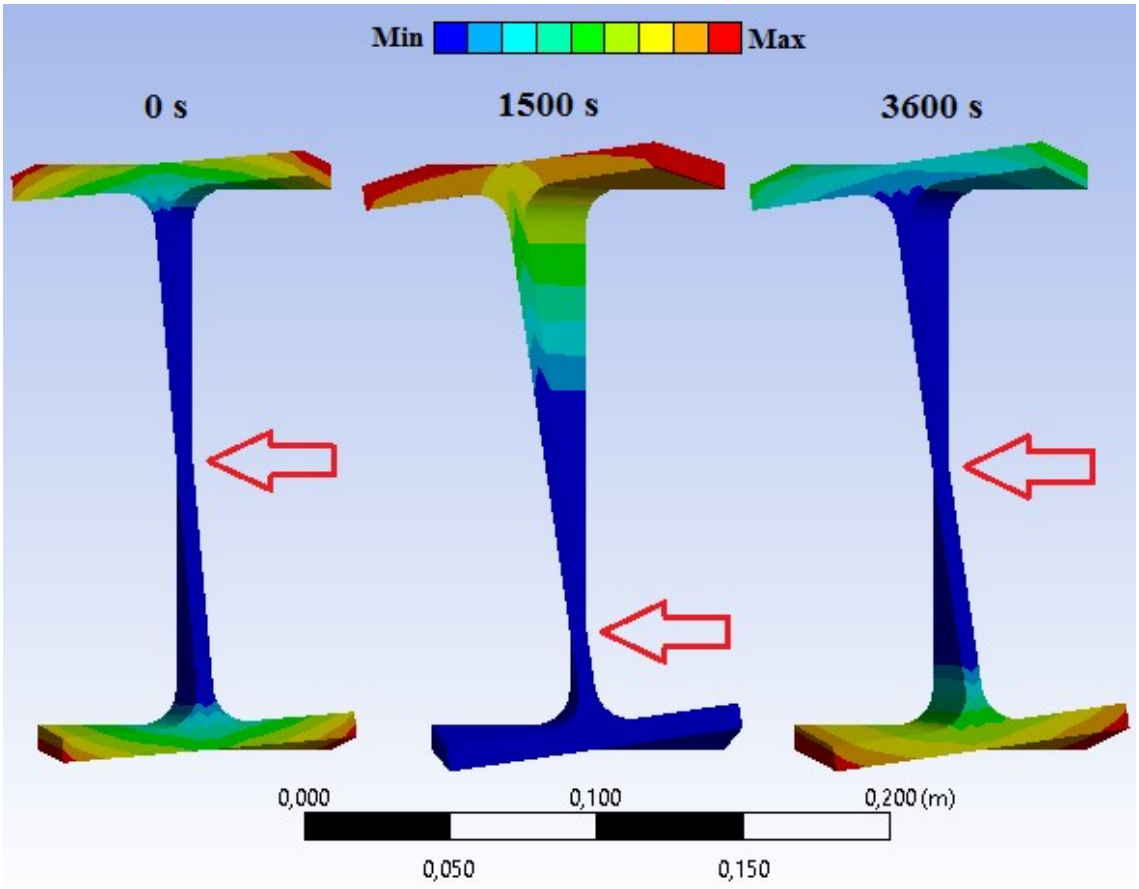

Figure 46. *Plastic strain of the partially protected IPE 200 beam at the start, middle and end of the fire [3]*

The dark blue colour indicates the areas of the cross section where plastic strain hasn't happened yet. As can be seen, at the beginning and end of the fire, where the yield strength of steel is relatively even across the cross section (see Figure 21), the plastic strain is spread rather evenly on the flanges of the beam, and the neutral axis (marked by the red arrow) is in the middle of the web. However, in the middle of the fire, where the differences in yield strength along the cross section are larger, most of the plastic strain happens at the unprotected flange, whereas the protected flange has no plastic strain at all. The heating time 1500 s was chosen to represent the plastic strain distribution in the middle of the fire because at that point in time the neutral axis was at its lowest point on the web.

6. CONCLUSIONS

The bending, shear and torsion resistances of two common open profiles were determined when the outer surface of the upper flange of the beam was unprotected. The other surfaces were covered with intumescent coating. The aim of this thesis was to provide the reader with heating time-resistance curves of a partially protected IPE 200 or HEA 200 beam to assist in designing steel structures.

The Eurocode does not cover active fire protection methods, and the offered methods for calculating bending, shear or torsion resistances for non-symmetrical temperature distributions are very limited. Therefore, tests or simulations must be performed to obtain these resistances when partially protecting a beam with intumescent coating. For this reason, three different FEM models were created for partially protected beams of both profile types, one for each loading case. These models were made for fully protected and unprotected beams as well to compare the results. The simulations were made using ANSYS Workbench. The material properties used for steel were from the Eurocode. The effective thermal conductivity of intumescent coating was calculated using a thermal expansion factor and a numerical approach by Schaumann et al. to determine the equivalent thermal conductivity of the coating. The other material properties of intumescent coating were from studies by Schaumann et al. and Tabeling. Thermal analyses were performed on all beams. The temperature distributions of the cross sections at different heating times were applied on the beams as body loads in structural analyses. The models were all cantilever beams with either a time-dependent rotation (for bending and torsion) or a time-dependent displacement (for shear) on the free end. The moment (bending and torsion) or force (shear) reactions on the supported end were measured as functions of the loading time. From these results the moment or force resistances of the beams at certain heating times were read when the plastic strain of the beams reached 0.2 %.

The temperature results of a 200 mm long fully protected IPE 200 beam were validated with simulation results by Schaumann et al. and test results by Tabeling. The steel temperature data of the present study showed great accordance when compared to the temperatures from both the simulation and the experiment. Due to the IPE 200 and HEA 200 profiles having such similar cross sections the HEA profile could be assumed to be validated as well.

The resistance results were plotted in heating time-resistance graphs for each profile type and loading case for all three levels of fire protection. The resulting resistance curves for bending, shear and torsion were all very similar in shape. For all loading cases the time it took to halve the resistance of a fully protected beam was generally about twice the time it took to halve the resistance of a partially protected beam. Similarly, the half time of the

resistance of a partially protected beam was roughly 1.5 times the half time of an unprotected beam. The half times of the HEA 200 profile were longer than the half times of the IPE 200 profile for all loading cases.

The results are clearly only applicable to IPE 200 and HEA 200 profiles. To expand the results to apply to a broader collection of cases further studies are required. One future research subject could be the effect of the size of the profile on the resistance curves (e.g. IPE 100, IPE 200, IPE 300 etc.). Another topic of interest is the effect of the initial thickness of the intumescent coating on the results. The loading cases studied could be expanded to include resistances to tension, buckling, and the combination of bending and shear. This study only covered open profiles, so the resistances of closed profiles would be a great topic for future research. Finally, in addition to all the simulations done on this study and mentioned here, tests should be performed to further verify the results.

REFERENCES

[1] Agarwal, A., Choe, L., Varma, A.H. Fire design of steel columns: Effects of thermal gradients. Journal of Constructional Steel Research 93(2014), pp. 107-118.

[2] Anderson, Jr., C.E., Ketchum, D.E., Mountain, W.P. Thermal conductivity of intumescent chars. Journal of Fire Sciences 6(1988)6, pp. 390-410.

[3] ANSYS Workbench, version 19.2, ANSYS, Inc.

[4] Baleshan, B., Mahendran, M. Fire design rules to predict the moment capacities of thin-walled floor joists subject to non-uniform temperature distributions. Thin-Walled Structures 105(2016), pp. 29-43.

[5] Bartholmai, M., Schartel, B. Assessing the performance of intumescent coatings using bench-scaled cone calorimeter and finite difference simulations. Fire and Materials 31(2007)3, pp. 187-205.

[6] BEAM188 Element Description [WWW]. [referenced 28.4.2019]. Available: https://www.sharcnet.ca/Software/Ansys/17.0/en-us/help/ans_elem/Hlp_E_BEAM188.html

[7] BEAM189 Element Description [WWW]. [referenced 28.4.2019]. Available: https://www.sharcnet.ca/Software/Ansys/17.0/en-us/help/ans_elem/Hlp_E_BEAM189.html

[8] Convection [WWW]. [referenced 28.4.2019] Available: https://www.sharcnet.ca/Software/Ansys/17.0/en-us/help/wb_sim/ds_Convection.html

[9] Dai, X., Wang, Y., Bailey, C. A simple method to predict temperatures in steel joints with partial intumescent coating fire protection. Fire Technology 46(2010)1, pp. 19-35.

[10] Dai, X.H., Wang, Y.C., Bailey, C.G. Effects of partial fire protection on temperature developments in steel joints protected by intumescent coating. Fire Safety Journal 44(2009)3, pp. 376-386.

[11] Dai, X.H., Wang, Y.C., Bailey, C.G. Numerical modelling of structural fire behaviour of restrained steel beam–column assemblies using typical joint types. Engineering Structures 32(2010)8, pp. 2337-2351.

[12] Di Blasi, C., Branca, C., Mathematical model for the nonsteady decomposition of intumescent coatings. AIChE Journal 47(2001)10, pp. 2359-2370.

[13] Feng, M., Wang, Y.C., Davies, J.M. Axial strength of cold-formed thin-walled steel channels under non-uniform temperatures in fire. Fire Safety Journal 38(2003)8, pp. 679-707.

[14] Griffin, G.J. The modeling of heat transfer across intumescent polymer coatings. Journal of Fire Sciences 28(2010)3, pp. 249-277.

[15] Griffin, G.J., Bicknell, A.D., Brown, T.J. Studies on the effect of atmospheric oxygen content on the thermal resistance of intumescent, fire-retardant coatings. Journal of Fire Sciences 23(2005)4, pp. 303-328.

[16] Guo, H., Long, X., Yao, Y. Fire resistance of concrete filled steel tube columns subjected to non-uniform heating. Journal of Constructional Steel Research 128(2017), pp. 542-554.

[17] Hautala, J., Pajunen, S., Mela, K., Heinisuo, M. Resistance of partially intumescent covered steel member in fire. 17th International Conference on Computing in Civil and Building Engineering, Tampere, Finland, June 5-7, 2018.

[18] Heinisuo, M., Jokinen, T. Tubular composite columns in a non-symmetrical fire. Magazine of Civil Engineering 49(2014)5, pp. 107-120.

[19] Horrocks, A.R. Developments in flame retardants for heat and fire resistant textiles-the role of char formation and intumescence. Polymer Degradation and Stability 54(1996)2, pp. 143-154.

[20] Kandola, B.K., Horrocks, S. Horrocks, A.R. Evidence of interaction in flame-retardant fibre-intumescent combinations by thermal analytical techniques. Thermochimica Acta 294(1997)1, pp. 113-125.

[21] Li, G-Q., Han, J., Lou, G-B., Wang, Y.C. Predicting intumescent coating protected steel temperature in fire using constant thermal conductivity. Thin-Walled Structures 98(2016), pp. 177-184.

[22] Li, G-Q., Lou, G-B., Zhang, C., Wang, L-L., Wang, Y-C. Assess the fire resistance of intumescent coatings by equivalent constant thermal resistance. Fire Technology 48(2012), pp. 529-546.

[23] Ma, Q., Wang, P., Huang, Q. Fire resistance of web-slotted cold-formed channel columns with non-uniform temperature distributions. Applied Mechanics and Materials 353-356(2013), pp. 2313-2318.

[24] Mao, C.H., Othuman Mydin, M.A., Que, X.B. Analytical model to establish the thermal conductivity of porous structure. Jurnal Teknologi 69(2014)1, pp. 103-111.

[25] Quiel, S.E., Garlock, M.E.M., Dwaikat, M.M.S., Kodur, V.K.R. Predicting the demand and plastic capacity of axially loaded steel beam–columns with thermal gradients. Engineering Structures 58(2014), pp. 49-62.

[26] Radiation [WWW]. [referenced 28.4.2019] Available: https://www.sharcnet.ca/Software/Ansys/17.0/en-us/help/wb_sim/ds_Radiation.html

[27] Salmi, T., Pajunen, S. Lujuusoppi. Tampere 2010, Pressus. 462 s.

[28] Schaumann, P., Tabeling, F., Weisheim, W. Fire design of steel structures with intumescent coatings. Nordic Steel Construction Conference, Tampere, Finland, September 23-25, 2015.

[29] Schaumann, P., Tabeling, F., Weisheim, W. Numerical simulation of the heating behaviour of steel profiles with intumescent coating adjacent to trapezoidal steel sheets in fire. Journal of Structural Fire Engineering 7(2016)2, pp. 158-167.

[30] SFS-EN 1991-1-2. Eurocode 1: Actions on structures. Part 1-2: General actions. Actions on structures exposed to fire. Helsinki 2003, Suomen Standardoimisliitto SFS ry. 61 p.

[31] SFS-EN 1993-1-1. Eurocode 3: Design of steel structures. Part 1-1: General rules and rules for buildings. Helsinki 2005, Suomen Standardoimisliitto SFS ry. 98 p.

[32] SFS-EN 1993-1-2. Eurocode 3: Design of steel structures. Part 1-2: General rules. Structural fire design. Helsinki 2005, Suomen Standardoimisliitto SFS ry. 82 p.

[33] SFS-EN 1993-1-5. Eurocode 3. Design of steel structures. Part 1-5: Plated structural elements. Helsinki 2006. Suomen Standardoimisliitto SFS ry. 55 p.

[34] Shahbazian, A., Wang, Y.C. Calculating the global buckling resistance of thin-walled steel members with uniform and non-uniform elevated temperatures under axial compression. Thin-Walled Structures 49(2011)11, pp.1415-1428.

[35] SOLID70 Element Description [WWW]. [referenced 28.4.2019] Available: https://www.sharcnet.ca/Software/Ansys/16.2.3/en-us/help/ans_elem/Hlp_E_SOLID70.html

[36] SOLID185 Element Description [WWW]. [referenced 28.4.2019] Available: https://www.sharcnet.ca/Software/Ansys/16.2.3/en-us/help/ans_elem/Hlp_E_SOLID185.html

[37] Staggs, J.E.J. Thermal conductivity estimates of intumescent chars by direct numerical simulation. Fire Safety Journal 45(2010), pp. 228-237.

[38] SURF152 Element Description [WWW]. [referenced 28.4.2019] Available: https://www.sharcnet.ca/Software/Ansys/17.0/en-us/help/ans_elem/Hlp_E_SURF152.html

[39] Tabeling, F. Zum Hochtemperaturverhalten dämmschichtbildender Brandschutzsysteme im Stahlbau (in English: High temperature behaviour of intumescent coating on steel constructions). Doctoral Thesis. Hannover 2014. Leibniz Universitaet Hannover. 312 p.

[40] Wang, P., Xia, J., Du, Q. Temperature rise of a protected steel column exposed to fire from two adjacent sides. Fire Technology 52(2016)6, pp. 1887-1914.

[41] Wang, Y., Göransson, U., Holmstedt, G., Omrane, A. A model for prediction of temperature in steel structure protected by intumescent coating, based on tests in the cone calorimeter. 8th International Symposium on Fire Safety Science, Beijing, China, September 18-23, 2005. pp. 235-246.

[42] Weil, E.D., Zhu, W., Patel, N., Mukhopadhyay, S.M. A systems approach to flame retardancy and comments on modes of action. Polymer Degradation and Stability 54(1996)2, pp. 125-136.

[43] Yang, H., Liu, F., Gardner, L. Performance of concrete-filled RHS columns exposed to fire on 3 sides. Engineering Structures 56(2013), pp. 1986-2004.

[44] Yang, H., Liu, F., Zhang, S., Lv, X. Experimental investigation of concrete-filled square hollow section columns subjected to non-uniform exposure. Engineering Structures 48(2013), pp. 292-312.

[45] Zhang, C. Reliability of steel columns protected by intumescent coatings subjected to natural fires. Doctoral Thesis. Berlin 2015. National Institute of Standards and Technology, USA. 140 p.

[46] Zhang, Y., Wang, Y.C., Bailey, C.G., Taylor, A.P. Global modelling of fire protection performance of intumescent coating under different cone calorimeter heating conditions. Fire Safety Journal 50(2012), pp. 51-62.

[47] Zhang, Y., Wang, Y.C., Bailey, C.G., Taylor, A.P. Global modelling of fire protection performance of an intumescent coating under different furnace fire conditions. Journal of Fire Sciences 31(2013)1, pp. 51-72.